174

HIGH PRESSURE ACADIAN METAMORPHISM OF THE STRAITS SCHIST, WESTERN CONNECTICUT

by

Stephen John Miller

Thesis submitted to the Faculty of the

Virginia Polytechnic Institute and State University

in partial fulfillment of the requirements for the degree of

MASTER OF SCIENCE

in

Geological Sciences

APPROVED:

Robert J. Tracy, Chairman

David A. Hewitt

Paul H. Ribbe

November, 1990

Blacksburg, Virginia

HIGH PRESSURE ACADIAN METAMORPHISM OF THE STRAITS SCHIST, WESTERN CONNECTICUT

by

Stephen John Miller

Committee Chairman: Robert J. Tracy
Geological Sciences

(ABSTRACT)

A detailed petrologic study of the maximum assemblage, minimum variance pelitic units contained within The Straits Schist in western Connecticut was undertaken to provide data on the Acadian Orogeny in the northern half of the western highlands of Connecticut. The Straits Schist, contained within the Connecticut Valley synclinorium, is structurally involved in portions of both the Hartland and Gneiss Dome belts, outlining isoclinally refolded nappes plunging off the Waterbury Dome. The Straits Schist is believed to be of Silurian–Devonian age, based on proposed correlations with the Goshen and the Waits River Formations of Massachusetts and Vermont, respectively. Furthermore, the age of metamorphism is interpreted as being Acadian based on the proposed age and stratigraphy, simple metamorphic textures, and uniform grain sizes. Quantitative estimates of the pressure and temperature conditions under which the mineral assemblages of The Straits Schist equilibrated were calculated using calibrated mineral reactions and ion exchange equilibria. Temperatures range from 607° – 747°C, and pressures range from 6.4 – 8.9 kbar across the study area. Estimates of P_{H_2O}/P_{total} were obtained and range between 0.21 and 0.57. Although exchange mechanisms have not (or could not have) been determined exactly , biotite and muscovite do show deviation from ideal tri- and di-octahedral stoichiometry, up to 13.7% dioctahedral character and 2.2% trioctahedral character, respectively. Compositional X-ray maps indicate that The Straits Schist underwent rapid

cooling. Therefore, the Acadian Orogeny in western Connecticut is characterized as a high pressure event that underwent rapid postmetamorphic uplift and cooling.

ACKNOWLEDGEMENTS

My sincerest and most heartfelt thanks are extended to my advisor, Dr. R.J. Tracy, for initially suggesting this research project to me and then providing me with advice, suggestions, guidance, and, most importantly, moral support. Thanks are also extended to Drs. D.A. Hewitt and P.H. Ribbe for giving helpful advice and suggestions concerning this project at various stages in its development. Dr. S.C. Eriksson is thanked for the use of her petrographic microscope. T.N. Solberg is gratefully acknowledged for his many late night hours of assistance in using the electron microprobe. S.S. Quarrier from the Connecticut Geological and Natural History Survey provided maps used in this study.

I would like to thank my parents, Carolyn and Michael, as well as my stepparents, Donald and Kathleen, for supporting me emotionally (and financially!!) throughout my life and for giving me the freedom to make my own decisions.

My brothers, David and Joseph, my sisters-in-law, Christi and Lynne, and my stepbrother, John, are acknowledged for their friendship and love. They kept telling me "I don't know exactly what you do in school, but as long as you are having fun, go for it!!" Well, I went for it.

My friends within Geological Sciences are many, and they are all thanked for their help and advice. There are, however, several individuals that deserve being mentioned by name. Bill Hames and Tom Armstrong are thanked for their many, many, many discussions concerning Appalachian regional geology. My sincerest thanks and debt of gratitude are owed to Tom Armstrong, Ann Schlinke, Ping Wang, Celia Clowe, Aditya Kar, Jeff Seitz, Carl Kirby, Mark Williamson, Barb Munn, Dave Winslow, Delpfine Welch, and Matt Nyman for keeping me sane. I truly could not have done it without you!!

My friends outside Geological Sciences are also thanked. You all have provided me with support and friendship that has made my tenure in Blacksburg some of the

happiest years of my life. The "Friends of Alice" group consisting (in part) of Jeff Trollinger and Rick Lemis, Dean Shaw and David Steyer, and Robert Lynch and David MacTavish are thanked for providing me with many good times and much laughter. Mark Zimmerman and Ken Nuss helped me through some rough times as well as many good times. Brian McConnell, Richard Brown, Aubrey Morgan, Paul Davenport, and many others whose names are too many to mention are also thanked for their friendship.

My deepest thanks are extended to Dirk Geratz for being my friend. Many times you have given me the willpower and energy to continue with school, and ultimately to finish my thesis. Thanks!!

My Washington, D.C. crowd of friends are also thanked for providing me with a much needed escape from Blacksburg. Jim Devaty and Dave Newhouse are especially thanked for their job hunting, apartment hunting, and "D.C. survival" help and advice. I also want to thank Jim for being a friend that occupies a special place in my heart, and I look forward to many more happy times together. Thanks!!

Funding was provided by the National Science Foundation grant EAR 88-16382 (to R.J. Tracy).

TABLE OF CONTENTS

LIST OF FIGURES

LIST OF TABLES

INTRODUCTION

An understanding of the full effects of each of the events that occurred over time is necessary to reconstruct the complete tectonometamorphic history of the eastern margin of North America. The Grenville Event (≈1100-1000 Ma), the Taconic Orogeny (≈475-445 Ma), the Acadian Orogeny (≈415-380 Ma), and the Alleghanian Orogeny (≈300-275 Ma) are the four events that have formed the northern Appalachians. This study was undertaken to provide data on one piece of tectonometamorphic history that shaped New England, that piece being the Acadian Orogeny in the northern half of the western highlands of Connecticut.

The Straits Schist in western Connecticut contains units of amphibolite, calc-silicate, marble, quartzite, and pelitic schist (Rodgers, 1985). Because of its mineral assemblages, the pelitic unit is of the most use in quantifying Acadian metamorphic conditions. This study has concentrated on the metamorphic history of The Straits Schist and has provided important information on the character of the Acadian Orogeny in western Connecticut and valuable input to a comprehensive model of the Acadian Orogeny in Southern and Central New England.

Prior to this work, a detailed petrologic study of The Straits Schist had not been undertaken. The Straits Schist is ideally suited for a detailed study for several reasons. First, whereas a pre-Acadian metamorphic history cannot be unequivocally ruled out, several pieces of evidence point to a single metamorphic event (see Geologic Setting - Age of Metamorphism, below). Second, this particular unit was chosen based on the mineral assemblages present. Mineral assemblages in pelitic rocks are highly useful for characterizing absolute conditions of metamorphism, based on many years of experimental

and field studies of pelitic assemblages. Relative changes in metamorphic grade can be traced through the mapping of metamorphic isograds. Isograds have been well documented in numerous regions throughout the world, and carefully interpreted isograds in metapelitic rocks have proven to be the most detailed and useful indicators of relative metamorphic grade.

The primary goal of this study was to characterize Acadian metamorphism in the northern half of the western highlands of Connecticut. This goal was achieved through detailed petrography and by obtaining a complete set of mineral chemistry data on The Straits Schist. These data were used to calculate pressures and temperatures which document the approximate peak metamorphic conditions to which The Straits Schist was subjected. In addition, an analysis of the continuous and/or discontinuous metamorphic reactions occurring in these pelites was undertaken in order to determine if the chemistry of the minerals is consistent with the prograde event, as well as to determine the range of metamorphic grades present.

GEOLOGIC SETTING

The Connecticut Valley synclinorium of the Iapetos (Oceanic) Terrane is bounded on the west by Cameron's Line and on the east by the Eastern border Fault (Rodgers, 1985). The Connecticut Valley synclinorium (alternatively, the Connecticut Valley - Gaspé synclinorium or the Connecticut Valley trough) extends for over 1000 km from Long Island Sound north through western Connecticut, western Massachusetts, eastern Vermont, northern New Hampshire, western Maine and through Québec to the tip of the Gaspé Peninsula (Hatch, 1988) (see Figure 1). Cameron's Line marks the westernmost extent of westward-thrusted allochthonous oceanic crust of the Taconian Orogeny (Rodgers, 1985). West of Cameron's Line the geology is dominated by Grenville-age (ca. 1100-1000 Ma) basement massifs of the rifted North American continental margin, overlain by autochthonous and parautochthonous lower Paleozoic sedimentary rocks. There are also scattered occurrences of far-traveled deep-water sedimentary rocks (the Taconic klippen) which are bounded below by Taconian-age thrust faults (Rodgers, 1985).

The Connecticut Valley synclinorium contains amphibolite-grade Lower to Middle Paleozoic clastic and volcaniclastic rocks that have been deformed and intruded by small granitic to dioritic plutons (Dietsch, 1989) overlying Taconian rocks (Stanley and Hatch, 1988). In Connecticut, the Connecticut Valley synclinorium is divided into three belts. The Hartland belt extends from Cameron's Line to a belt in the eastern portion of the Connecticut Valley synclinorium west of the Hartford Basin (see Figure 2) which contains a series of domes and is therefore called the Gneiss Dome belt. Three domes (the Granville, Collinsville, and Bristol Domes) are in contact with rocks of the Hartford

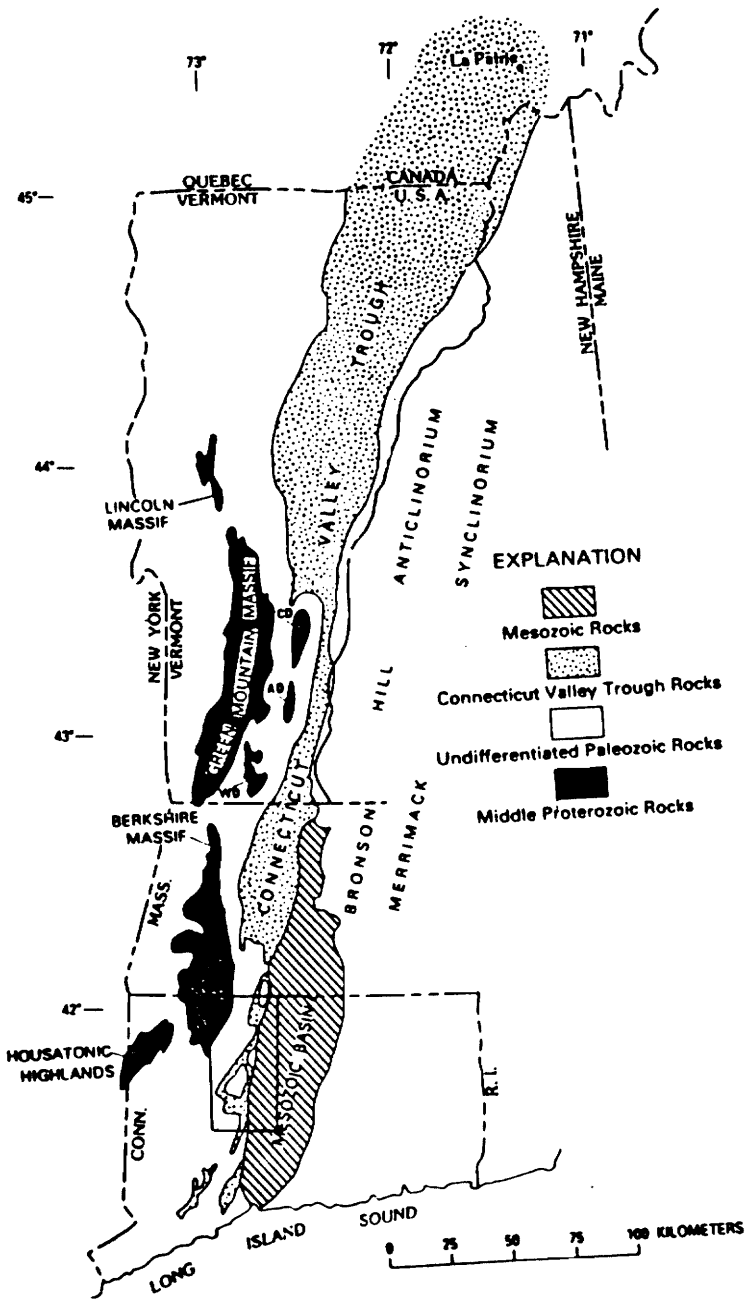

Figure 1. Map of western New England showing the location of the Connecticut Valley Trough (Connecticut Valley synclinorium) in relation to other geologic features. CD is the Chester dome, AD is the Athens dome, and WD is the Wilmington dome. After Hatch (1988). Boxed region is approximate area of Figures 3, 8, 9, and 10.

Figure 2. Simplified geologic map of western Connecticut (modified from Dietsch, 1988 after Rodgers, 1982, 1985). The ages of rocks exposed in the domes is uncertain. Boxed region is approximate area of Figures 3, 8, 9, and 10.

Explanation

Mz	Mesozoic rocks
S-D	Silurian-Devonian rocks; with fine stipple, The Straits Schist
O	Ordovician Rocks
OZ	Ordovician-Proterozoic Z rocks
C-O	Cambrian-Ordovician rocks
C-Z	Cambrian-Proterozoic Z rocks; with coarse stipple rocks of the Taconic Allochthons
Y	Proterozoic Y rocks
Yb, Yho, Yhd	Proterozoic Y rocks of the Berkshire (Yb) massif, Housatonic (Yho) massif, and the Hudson (Yhd) Highlands

Intrusive rocks

Dg	Devonian granitic rocks
Om	Ordovician intermediate, mafic, and ultramafic rocks
Og	Ordovician granitic rocks

Structures

CL	Cameron's Line
	normal faults shown as unlabelled heavy lines

Domes

GD	Granville
GbD	Granby
CD	Collinsville
BD	Bristol
WD	Waterbury

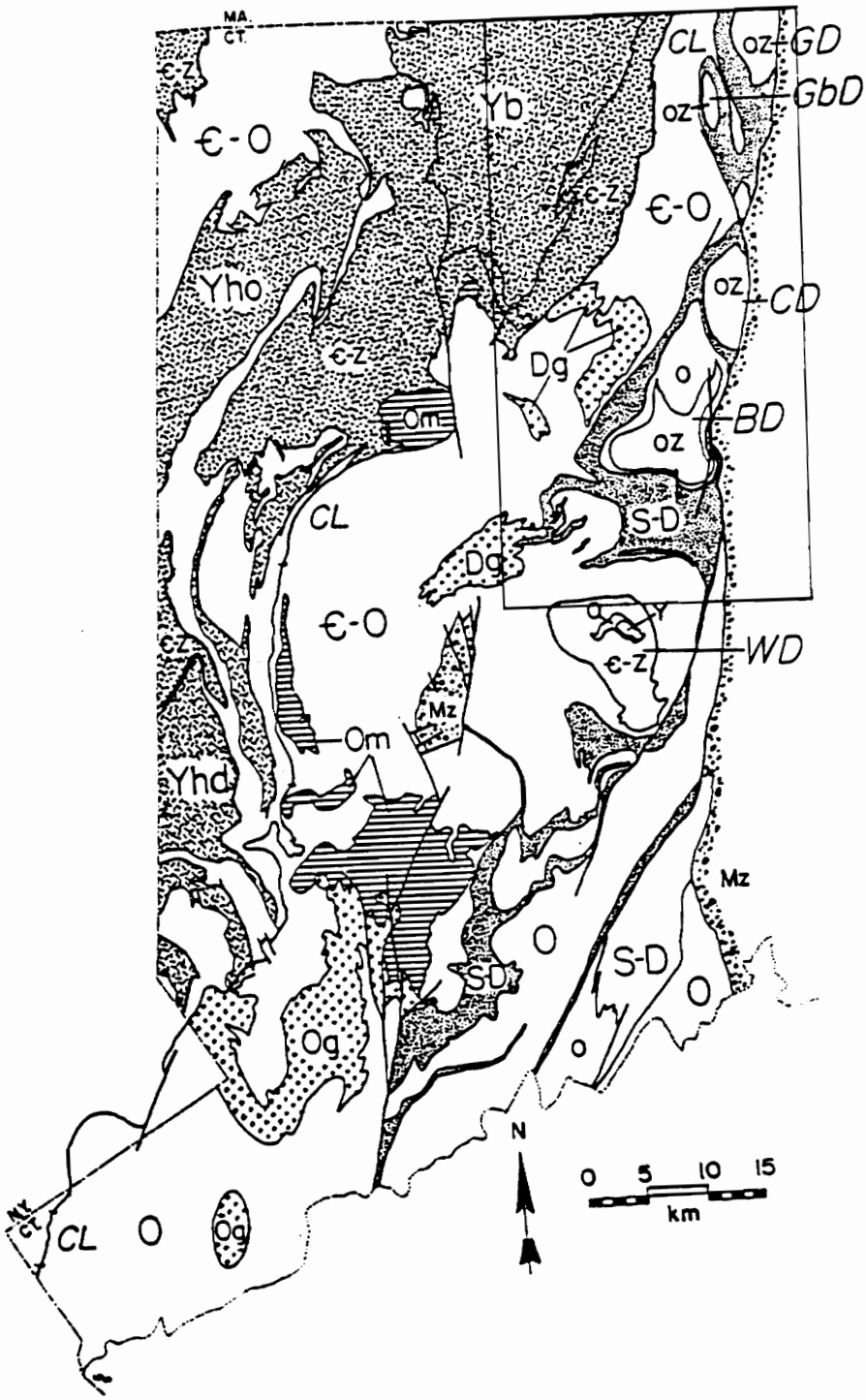
MA.
CT.
NY
CT.
€-Z
€-O
Yb
Yho
Yhd
Om
CL
Dg
Mz
Og
O
S-D
oz
GD
GbD
CD
BD
WD
o
N
0 5 10 15
km

Mesozoic Basin, whereas two others (the Granby and Waterbury Domes) are slightly to the west of the other three domes. The Straits Schist is structurally involved in portions of both the Hartland and Gneiss Dome belts, outlining isoclinally refolded nappes plunging off the Waterbury Dome (Dietrich, 1968).

The third belt, the Orange-Milford belt, occupies a relatively small area west and northwest of New Haven, and is bounded by the East Derby Fault to the west and by the Hartford Basin and Long Island Sound to the east and south, respectively. This belt consists of greenschist- to amphibolite-grade rocks (Fritts, 1962; Rodgers, 1985). The Wepawaug Schist is a major lithologic constituent of this belt and may be correlative with The Straits Schist (Rodgers, 1985). The Bronson Hill anticlinorium and Merrimac synclinorium lie to the east of the Hartford Basin and are also members of the Iapetos (Oceanic) Terrane. Late Precambrian granites and gneisses of the Avalonian (Continental) Terrane are exposed to the south and east of the Bronson Hill anticlinorium and Merrimac synclinorium (Rodgers, 1985).

PREVIOUS WORK

Age and Stratigraphic Correlations

Much debate has taken place over the age and stratigraphic correlations of The Straits Schist. Originally described by Silliman (1820) as "mica-slate with garnets and staurotide" and later defined as a member of the Hartland Formation by Rodgers and others (1959), The Straits Schist was raised to formational rank by Fritts (1962, 1963). Fritts (1962) assigned a Cambrian*(?)* age based on its petrologic and structural similarity to the Early Cambrian*(?)* Hoosac Formation of Massachusetts and Vermont. Stanley (1968),

Hatch and Stanley (1973), Hall (1976), Rodgers (1985), and many other workers correlated The Straits Schist with the Goshen Formation of Massachusetts. Most recently, Hatch (1988) correlated The Straits Schist with the Goshen Formation as well as with the Waits River Formation of Vermont. The most widely accepted age for The Straits Schist is Silurian - Devonian, based on the proposed correlations with the Goshen and the Waits River Formations.

Age of Metamorphism

Based on his observation that The Straits is characterized by simple textures and uniform grain size, Fritts (1962) concluded that it probably underwent progressive regional metamorphism only once. Nearby to the west, pre-Silurian rocks show petrographic evidence which indicates both Taconian and Acadian progressive metamorphism (Hames, 1990). Muscovite and biotite K-Ar ages from Clark and Kulp (1968), Seidemann (1980), and Armstrong and others (1970) are in the range 337-370 Ma, indicative of post-Acadian metamorphic cooling ages. Hornblende K-Ar ages of Clark and Kulp (1968) in the range 366-396 Ma again indicate Acadian metamorphism.

Many workers have tried to determine the age of The Straits Schist and its correlative units using structural, stratigraphic, and paleontological arguments (see references in Hatch, 1988). Hatch (1988, p. 1056) stated "the [Connecticut Valley] trough rocks appear to be constrained to the time interval between the Taconian and Acadian orogenies." Stanley and Hatch (1988) provided stratigraphic and structural evidence that The Straits Schist was involved in only one metamorphic event. They correlated The Straits Schist with the Goshen Formation in Massachusetts which lies conformably above the Russell Mountain Formation, and called these formations members of the Connecticut

Valley Belt (CVB). The CVB unconformably overlies the Rowe-Hawley Zone, which is a belt containing Taconian synmetamorphic thrust faults that are truncated by rocks of the CVB. This sequence therefore places the deposition of the CVB above (younger than) the Taconian thrust faults, thereby making the age of The Straits Schist post-Taconian.

Following the Acadian Orogeny, there is no evidence of heating above ≈300-350°C (approximate mica closure temperature). This indicates that effects of the Alleghanian Orogeny on The Straits Schist, if any, were minor or insignificant because there was no resetting of the muscovite or biotite K-Ar ages (Dietsch, 1988).

The evidence discussed above indicates that The Straits Schist underwent a single progressive regional metamorphism. This gives rise to the conclusion that a detailed petrologic analysis of The Straits Schist is, in essence, an analysis of Acadian metamorphism in southwestern New England.

PETROGRAPHY AND MINERAL CHEMISTRY

Samples were collected by R.J. Tracy in 1987 and 1988, largely from recent man-made exposures in an attempt to obtain a wide distribution of the freshest possible samples. Sample locations for these rocks are shown on Figure 3. Twelve of the thirty thin sections examined were deemed suitable for determining both pressures and temperatures because they have the critical assemblage biotite + garnet + plagioclase + ilmenite + rutile + kyanite/sillimanite + quartz. Three samples (BR-2, TH-13, and WAT-3) have an assemblage suitable for a temperature determination only (biotite + garnet + plagioclase + rutile + quartz, lacking ilmenite and/or aluminum silicate).

PETROGRAPHY

Petrography was done on polished thin sections. All the sections chosen for probe analyses were point counted (at least 500 points per sample). Table 1 lists assemblages, modes, and mineral abbreviations. The following petrographic descriptions are for the thirteen thin sections chosen for detailed petrologic study. These descriptions can be applied to all the thin sections examined, save minor variations in mineral assemblages.

The Straits Schist is a medium- to coarse-grained plagioclase - biotite - muscovite - quartz schist with a lepidoblastic texture containing porphyroblasts of garnet, kyanite (two samples contain sillimanite or fibrolite), and locally staurolite. Accessory minerals include rutile, ilmenite, tourmaline, apatite, monazite, sericite, chlorite, and graphite. Many samples contain lensoid segregations of coarse, equant quartz and plagioclase.

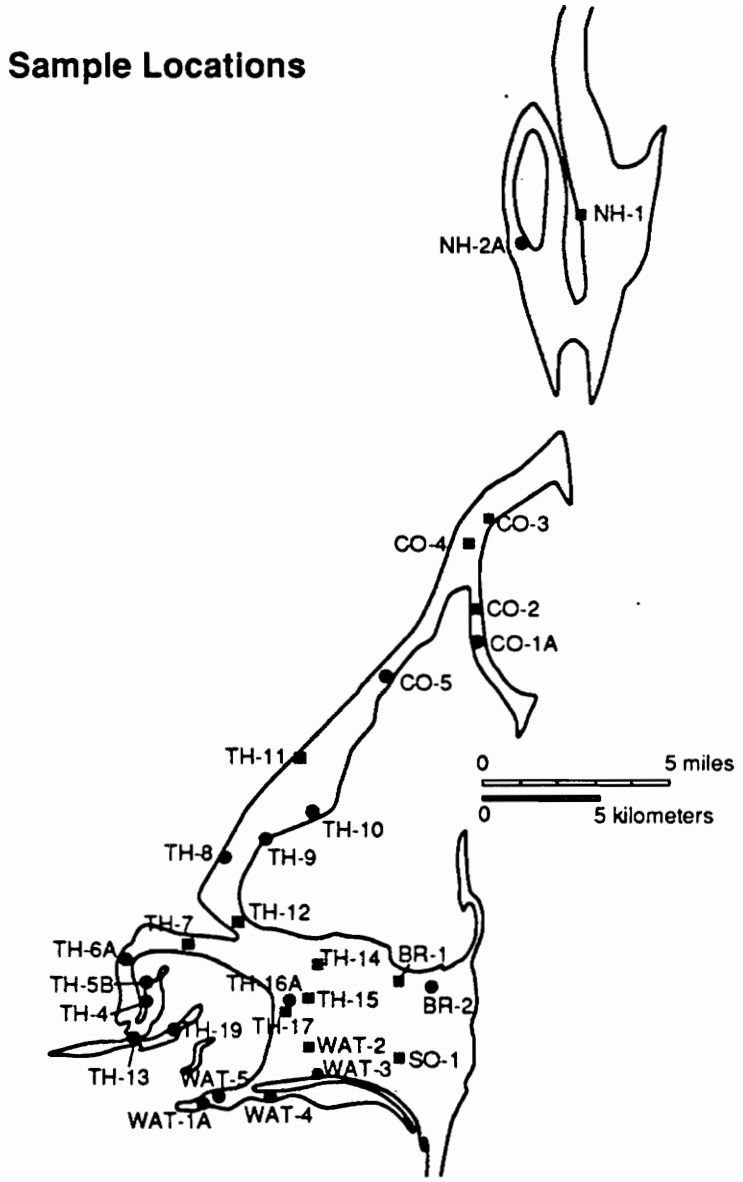

Figure 3. Simplified geologic map showing sample locations. Solid circles represent samples analyzed by electron microprobe. Solid squares represent samples that have only had petrographic analyses.

Table 1. Assemblages, modes and mineral abbreviations

	BR-2	CO-1A	CO-5	NH-2A	TH-4	TH-5B	TH-6A	TH-8	TH-9	TH-10	TH-13
quartz (Qtz)	11.9	25.0	35.4	16.1	47.3	50.7	49.1	48.3	31.1	42.6	43.2
plagioclase (Pl)	0.9	1.2	7.1	22.2	4.6	7.2	6.8	5.7	7.1	10.2	1.5
biotite (Bt)	23.6	20.3	19.0	29.3	13.0	28.4	14.2	21.8	11.9	10.4	14.9
muscovite (Ms)	42.9	41.0	25.6	26.2	27.5	7.6	22.6	19.2	30.2	26.4	33.0
garnet (Grt)	11.1	10.9	5.2	5.2	6.0	4.0	6.4	2.4	17.6	8.0	6.8
kyanite (Ky)	–	0.7	6.4	0.2	1.4	0.7	0.4	1.4	1.4	2.1	–
sillimanite (Sil)	–	–	–	0.4[f]	–	–	–	–	–	–	–
staurolite (St)	6.6	0.4	x	–	–	0.1	x	0.4	0.5	0.3	0.2
ilmenite (Ilm)	0.9	x	0.4	x	x	0.1	–	x	0.2	x	–
rutile (Rt)	0.3	0.4	0.6	0.4	0.3	0.1	0.2	0.4	0.2	x	0.4
tourmaline (Tur)	1.9	–	x	–	x	0.4	0.2	0.3	–	–	x
chlorite (Chl)	x	–	x	x	x	–	x	–	–	–	–
monazite (Mnz)	x	x	x	x	x	0.1	x	x	x	x	x
opaques*	x	x	x	x	x	x	x	x	x	x	x
graphite (Gr)	–	–	–	x	–	0.3	x	–	–	–	x
apatite (Ap)	x	x	0.3	x	x	x	x	x	x	x	x

	TH-16A	TH-19	WAT-1A	WAT-3	WAT-4	WAT-5	SO-1	CO-2	CO-3	CO-4	BR-1
quartz	44.4	33.8	35.8	34.0	35.3	40.3	x	x	x	x	x
plagioclase	7.8	11.6	7.4	5.2	5.5	12.5	x	x	x	x	x
biotite	23.4	23.1	18.4	14.3	15.9	15.7	x	x	x	x	x
muscovite	15.4	23.1	27.2	31.4	27.7	25.2	x	x	x	x	x
garnet	2.5	3.9	7.4	11.0	8.1	3.1	x	x	x	x	x
kyanite	–	4.5	2.3	3.4	5.7	2.3	–	x	x	x	–
sillimanite	5.7	–	–	–	–	–	–	–	–	–	–
staurolite	–	–	0.4	0.2	0.3	0.2	x	x	–	–	x
ilmenite	0.3	x	x	–	x	0.8	–	–	–	–	–
rutile	0.3	x	0.5	0.2	0.5	x	x	x	x	–	x
tourmaline	–	–	–	0.2	–	x	x	–	–	x	x
chlorite	–	–	–	–	–	x	–	x	x	–	–
monazite	x	x	x	x	0.1	x	x	x	x	x	x
opaques*	x	x	x	x	x	x	x	x	x	x	x
graphite	0.2	–	0.5	x	0.9	–	–	–	–	–	x
apatite	x	x	x	x	x	x	x	x	x	x	x

Table 1 (continued). Assemblages, modes and mineral abbreviations

	NH-1	TH-7	TH-11	TH-12	TH-14	TH-15	TH-17	WAT-2
quartz	x	x	x	x	x	x	x	x
plagioclase	x	x	x	x	x	x	x	x
biotite	x	x	x	x	x	x	x	x
muscovite	x	x	x	x	x	x	x	x
garnet	x	x	x	x	x	x	x	x
kyanite	–	–	x	–	–	–	–	–
sillimanite	–	–	–	–	–	–	–	–
staurolite	–	–	x	–	x	x	x	x
ilmenite	–	–	–	–	–	–	–	–
rutile	x	x	x	x	–	x	x	x
tourmaline	–	x	x	x	x	x	x	x
chlorite	–	x	x	–	–	–	–	x
monazite	x	x	x	x	x	x	x	x
opaques*	x	x	x	x	x	x	x	x
graphite	–	–	–	–	–	–	–	–
apatite	x	x	x	x	x	x	x	x

* including pyrrhotite (Po), chalcopyrite (Ccp), and magnetite (Mag)
x = present
-- = not present
f = fibrolitic variety

Quartz has mosaic, undulatory, or relatively uniform extinction. Plagioclase may or may not exhibit albite twinning, and ranges in composition between approximately An_{13} and An_{29}. Plagioclase shows some alteration to sericite, and may contain inclusions of quartz.

Garnet is present as poikiloblastic anhedral to euhedral grains, with inclusions of quartz, plagioclase, biotite, and opaques typically, although not always, concentrated in the core. Inclusions in garnet may form an alignment parallel or at an angle to the external foliation, or have an S-shape indicative of rotation of the garnet during growth (Yardley, 1989). Some garnets are sievelike. Many of the garnets are fractured and broken. At least two garnets have compositional zoning patterns indicating the garnets have been broken, and furthermore show very minor reequilibration effects (see Figures 4d and 5d). Garnets range in size from about 0.5 to 5 mm.

Micas are commonly aligned in layers defining the lepidoblastic texture. Muscovite is typically coarse grained, although fine grained muscovite may be found with or without the coarse variety. Biotites are strongly pleochroic, from pale brown to dark brown or dark red. Graphite may or may not be present; when present, it is aligned parallel to the mica grains.

Small to large (up to ≈1 cm) kyanite blades are present in most of the thin sections chosen for detailed petrographic work. Many of the kyanite grains are altered to sericite while others show little alteration. Typically, the kyanite blades are aligned parallel to the foliation, but this is not always the case. One thin section (TH-16A) contains prismatic sillimanite, and sample NH-2A contains both kyanite and matted fibrolite.

Staurolite occurs in select samples as anhedral to euhedral, nonpoikiloblastic to sievelike porphyroblasts displaying a wide degree of size variation. Several grains have a

resorbed appearance. Some grains exhibit alteration to sericite. Staurolites are pale to dark yellow color and most exhibit strong pleochroism.

MINERAL CHEMISTRY

The chemical compositions of muscovite, biotite, garnet, plagioclase, ilmenite, and staurolite in all samples were analyzed by electron microprobe. All the microprobe analyses were made on polished thin sections using a CAMECA SX-50 fully automated electron microprobe at Virginia Polytechnic Institute and State University. Operating conditions were 15 keV accelerating potential and either 20 nA beam current (for garnet, ilmenite, and staurolite) or a 10 nA beam current (for muscovite, biotite, and plagioclase). Standardization was done with natural and synthetic standards, and was periodically checked using a mineral of known composition not involved in the standardization procedure. Table 2 lists the standards for mineral analyses. Data were reduced using ZAF corrections (Heinrich, 1981, chapters 8-12).

Mineral formulas and compositions are given in Table 3 for muscovite, in Table 4 for biotite, in Table 5 for garnet, in Table 6 for plagioclase, in Table 7 for ilmenite, and in Table 8 for staurolite. Muscovite and biotite formulas were calculated on an anhydrous formula basis of eleven oxygens. For garnet, formulas are based on charge balance for twelve oxygens. Plagioclase formulas are based on eight oxygens, ilmenite formulas are based on three oxygens, and staurolite formulas are based on forty-eight oxygens.

Muscovite

The dioctahedral white micas can be described in terms of four compositional end-members:

Table 2. Standards Used in Mineral Analyses

Oxide	Standard
SiO_2	albite
TiO_2	rutile
Al_2O_3	albite
FeO	hematite or fayalite
MnO	pyrolusite
MgO	periclase
ZnO	willemite
CaO	wollastonite
Na_2O	albite
K_2O	orthoclase
F	norbergite
Cl	Ca_2PO_4Cl

Muscovite	$KAl_2AlSi_3O_{10}(OH)_2$
Paragonite	$NaAl_2AlSi_3O_{10}(OH)_2$
Margarite	$CaAl_2Al_2Si_2O_{10}(OH)_2$
Celadonite	$(K,Na)Al(Fe,Mg)Si_4O_{10}(OH)_2$.

These end members are derived by isomorphous simple or coupled substitutions preserving charge balance and dioctahedral stoichiometry (Deer and others, 1966; Tracy, 1978). Structural formulas shown in Table 3 indicate a slight deviation from ideal dioctahedral stoichiometry. The sum of octahedral cations ranges between 2.020 and 2.044, with a mean of 2.031. Substitution mechanisms will be examined in the Discussion.

Muscovites in this study show extensive replacement of K by Na in the interlayer site (up to ≈23 mol % paragonite). Muscovites from The Straits Schist show virtually no substitution by Ca, which is consistent with observations made of metamorphic muscovites by Evans and Guidotti (1966), Guidotti (1973), and Tracy (1978). The muscovites contain so little F and Cl that the substitution of F and Cl for (OH) is insignificant.

Biotite

Most trioctahedral dark micas can be described in terms of four biotite end-members:

Phlogopite	$KMg_3AlSi_3O_{10}(OH)_2$
Annite	$KFe_3^{2+}AlSi_3O_{10}(OH)_2$
Eastonite	$KMg_{2.5}Al_{0.5}Al_{1.5}Si_{2.5}O_{10}(OH)_2$
Siderophyllite	$KFe_{2.5}Al_{0.5}Al_{1.5}Si_{2.5}O_{10}(OH)_2$.

The composition of biotite can deviate considerably from the theoretical biotite end-members. Common cation substitutions involve replacement of Mg^{2+} and Fe^{2+} by Al^{3+},

Table 3. Microprobe Analyses of Muscovites

	BR-2	CO-1A	CO-5	NH-2A	TH-4	TH-5B	TH-6A	TH-8
SiO_2	46.17	46.54	45.47	46.94	45.99	46.32	46.80	46.09
TiO_2	0.59	0.86	0.98	1.04	0.73	0.77	0.79	0.87
Al_2O_3	36.58	36.21	34.88	34.33	36.52	35.64	35.58	36.01
FeO	0.92	1.17	1.14	1.33	1.06	1.05	1.02	1.16
MnO	0.03	0.01	0.02	0.00	0.04	0.01	0.02	0.01
MgO	0.62	0.69	0.69	1.16	0.72	0.88	0.78	0.70
CaO	0.02	0.02	0.02	0.02	0.01	0.02	0.02	0.01
Na_2O	1.72	1.17	1.26	0.84	1.28	1.23	1.14	1.44
K_2O	8.61	9.36	9.11	9.52	8.89	9.03	9.26	9.11
F	0.06	0.09	0.03	0.06	0.06	0.09	0.06	0.04
Cl	0.02	0.01	0.00	0.01	0.01	0.01	0.01	0.01
total	95.34	96.13	93.60	95.25	95.31	95.05	95.48	95.45
-O=F+Cl	0.03	0.04	0.01	0.03	0.03	0.04	0.03	0.02
total	95.31	96.09	93.59	95.22	95.28	95.01	95.45	95.43

Anhydrous formulas calculated on the basis of 11 oxygens

Si	3.043	3.053	3.065	3.111	3.035	3.067	3.085	3.046
Al	0.957	0.947	0.935	0.889	0.965	0.933	0.915	0.954
	4.000	4.000	4.000	4.000	4.000	4.000	4.000	4.000
Al	1.884	1.853	1.836	1.792	1.876	1.848	1.850	1.850
Ti	0.029	0.042	0.050	0.052	0.036	0.038	0.039	0.043
Fe	0.051	0.064	0.064	0.074	0.059	0.058	0.056	0.064
Mn	0.002	0.001	0.001	0.000	0.002	0.001	0.001	0.001
Mg	0.061	0.067	0.069	0.115	0.071	0.087	0.077	0.069
	2.027	2.027	2.020	2.033	2.044	2.032	2.026	2.027
Ca	0.001	0.001	0.001	0.001	0.001	0.001	0.001	0.001
Na	0.220	0.149	0.165	0.108	0.164	0.158	0.146	0.184
K	0.724	0.783	0.783	0.805	0.749	0.763	0.779	0.768
	0.945	0.933	0.949	0.914	0.914	0.922	0.926	0.954
F	0.013	0.019	0.006	0.013	0.013	0.019	0.013	0.008
Cl	0.002	0.001	0.000	0.001	0.001	0.001	0.001	0.001
	0.015	0.020	0.006	0.014	0.014	0.020	0.014	0.009
K/K+Na+Ca	0.766	0.839	0.825	0.880	0.820	0.827	0.841	0.806
Na/K+Na+Ca	0.233	0.159	0.173	0.118	0.179	0.171	0.157	0.194
Ca/K+Na+Ca	0.002	0.002	0.002	0.002	0.001	0.002	0.002	0.001
Fe/Fe+Mg	0.454	0.488	0.481	0.391	0.452	0.401	0.432	0.482

Table 3. (continued) Microprobe Analyses of Muscovites

	TH-9	TH-10	TH-16A	TH-19	WAT-1A	WAT-4	WAT-5
SiO_2	46.03	45.93	45.83	46.31	46.60	46.05	46.78
TiO_2	0.93	0.90	0.87	0.86	0.50	0.35	0.91
Al_2O_3	35.02	35.42	35.17	34.65	36.95	37.11	35.42
FeO	1.32	1.28	1.24	1.18	0.98	1.06	1.19
MnO	0.02	0.02	0.01	0.05	0.00	0.01	0.02
MgO	0.87	0.82	0.69	1.08	0.61	0.46	0.95
CaO	0.01	0.03	0.01	0.01	0.02	0.02	0.01
Na_2O	1.19	1.32	1.35	1.10	1.20	1.34	1.25
K_2O	9.08	9.09	9.05	9.54	9.07	8.96	9.04
F	0.06	0.07	0.06	0.04	0.07	0.06	0.05
Cl	0.02	0.01	0.00	0.00	0.03	0.01	0.01
total	94.55	94.89	94.28	94.82	96.03	95.43	95.63
-O=F+Cl	0.03	0.03	0.03	0.02	0.04	0.03	0.02
total	94.52	94.86	94.25	94.80	95.99	95.40	95.61
Anhydrous formulas calculated on the basis of 11 oxygens							
Si	3.071	3.055	3.066	3.087	3.049	3.034	3.080
Al	0.929	0.945	0.934	0.913	0.951	0.966	0.920
	4.000	4.000	4.000	4.000	4.000	4.000	4.000
Al	1.825	1.832	1.840	1.809	1.899	1.916	1.829
Ti	0.047	0.045	0.044	0.043	0.025	0.017	0.045
Fe	0.074	0.071	0.069	0.066	0.054	0.058	0.066
Mn	0.001	0.001	0.001	0.003	0.000	0.001	0.001
Mg	0.087	0.081	0.069	0.107	0.060	0.045	0.093
	2.034	2.030	2.023	2.028	2.038	2.037	2.034
Ca	0.001	0.002	0.001	0.001	0.001	0.001	0.001
Na	0.154	0.170	0.175	0.142	0.152	0.171	0.160
K	0.773	0.771	0.772	0.811	0.757	0.753	0.759
	0.928	0.943	0.948	0.954	0.910	0.925	0.920
F	0.013	0.015	0.013	0.008	0.014	0.013	0.010
Cl	0.002	0.001	0.000	0.000	0.003	0.001	0.001
	0.015	0.016	0.013	0.008	0.017	0.014	0.011
K/K+Na+Ca	0.833	0.817	0.815	0.850	0.831	0.814	0.826
Na/K+Na+Ca	0.166	0.180	0.185	0.149	0.167	0.185	0.174
Ca/K+Na+Ca	0.001	0.002	0.001	0.001	0.002	0.002	0.001
Fe/Fe+Mg	0.460	0.467	0.502	0.380	0.474	0.564	0.413

Table 4. Microprobe Analyses of Biotites

	BR-2	CO-1A	CO-5	NH-2A	TH-4	TH-5B	TH-6A	TH-8	TH-9
SiO_2	35.58	36.08	34.67	36.43	35.07	35.62	35.58	35.50	34.83
TiO_2	1.51	1.89	2.39	1.70	1.80	1.86	1.84	2.27	2.23
Al_2O_3	19.70	20.15	19.11	20.49	19.76	19.9	19.99	19.56	19.19
FeO	22.54	20.96	22.44	19.71	21.19	19.76	21.76	19.51	23.14
MnO	0.07	0.02	0.05	0.05	0.07	0.06	0.03	0.10	0.05
MgO	8.91	9.61	8.70	10.25	9.30	9.92	9.57	10.11	8.27
CaO	0.01	0.00	0.01	0.04	0.00	0.02	0.02	0.03	0.02
Na_2O	0.12	0.27	0.32	0.23	0.29	0.29	0.23	0.38	0.13
K_2O	8.22	8.32	7.85	8.27	7.92	8.02	7.96	8.40	8.42
F	0.26	0.24	0.19	0.25	0.20	0.22	0.18	0.22	0.24
Cl	0.02	0.01	0.01	0.03	0.01	0.01	0.02	0.00	0.01
total	96.94	97.55	95.74	97.45	95.61	95.68	97.18	96.08	96.53
-O=F+Cl	0.11	0.10	0.08	0.11	0.09	0.09	0.08	0.09	0.10
total	96.83	97.45	95.66	97.34	95.52	95.59	97.10	95.99	96.43
Anhydrous formulas calculated on the basis of 11 oxygens									
Si	2.676	2.673	2.646	2.682	2.659	2.677	2.656	2.664	2.650
Al	1.324	1.327	1.354	1.318	1.341	1.323	1.344	1.336	1.350
	4.000	4.000	4.000	4.000	4.000	4.000	4.000	4.000	4.000
Al	0.422	0.433	0.365	0.460	0.425	0.440	0.414	0.394	0.371
Ti	0.085	0.105	0.137	0.094	0.103	0.105	0.103	0.128	0.128
Fe	1.418	1.299	1.432	1.214	1.344	1.242	1.358	1.224	1.472
Mn	0.004	0.001	0.003	0.003	0.004	0.004	0.002	0.006	0.003
Mg	0.999	1.062	0.990	1.125	1.051	1.111	1.065	1.131	0.938
	2.928	2.900	2.927	2.896	2.927	2.902	2.942	2.883	2.912
Ca	0.001	0.000	0.001	0.003	0.000	0.002	0.002	0.002	0.002
Na	0.017	0.039	0.047	0.033	0.043	0.042	0.033	0.055	0.019
K	0.789	0.786	0.764	0.777	0.766	0.769	0.758	0.804	0.817
	0.807	0.825	0.812	0.813	0.809	0.813	0.793	0.861	0.838
F	0.062	0.056	0.046	0.058	0.048	0.052	0.042	0.052	0.058
Cl	0.003	0.001	0.001	0.004	0.001	0.001	0.003	0.000	0.001
	0.065	0.057	0.047	0.062	0.049	0.053	0.045	0.052	0.059
Fe/Fe+Mg	0.587	0.550	0.591	0.519	0.561	0.528	0.561	0.520	0.611

Table 4, (continued) Microprobe Analyses of Biotites

	TH-10	TH-13	TH-16A	TH-19	WAT-1A	WAT-3	WAT-4	WAT-5
SiO_2	35.38	35.09	35.30	35.94	35.49	34.56	36.09	35.12
TiO_2	1.54	2.24	2.52	2.23	2.43	1.94	2.55	2.48
Al_2O_3	20.14	19.35	19.15	19.81	19.78	19.03	19.66	19.64
FeO	21.53	22.96	22.46	18.56	21.38	21.23	21.59	21.76
MnO	0.06	0.06	0.04	0.12	0.05	0.04	0.04	0.06
MgO	9.23	8.29	8.08	10.59	8.81	9.22	9.10	8.98
CaO	0.02	0.00	0.01	0.01	0.02	0.05	0.04	0.02
Na_2O	0.31	0.29	0.34	0.28	0.35	0.25	0.25	0.27
K_2O	8.33	7.86	8.19	8.87	8.23	7.74	8.77	7.94
F	0.23	0.19	0.18	0.29	0.18	0.19	0.18	0.19
Cl	0.01	0.02	0.00	0.02	0.03	0.01	0.01	0.02
total	96.78	96.35	96.27	96.72	96.75	94.26	98.28	96.48
-O=F+Cl	0.10	0.08	0.08	0.13	0.08	0.08	0.08	0.08
total	96.68	96.27	96.19	96.59	96.67	94.18	98.20	96.40

Anhydrous formulas calculated on the basis of 11 oxygens

Si	2.656	2.662	2.679	2.670	2.663	2.663	2.672	2.646
Al	1.344	1.338	1.321	1.330	1.337	1.337	1.328	1.354
	4.000	4.000	4.000	4.000	4.000	4.000	4.000	4.000
Al	0.439	0.393	0.391	0.404	0.413	0.391	0.387	0.390
Ti	0.087	0.128	0.144	0.125	0.137	0.112	0.142	0.141
Fe	1.352	1.457	1.425	1.153	1.342	1.368	1.337	1.371
Mn	0.004	0.004	0.003	0.008	0.003	0.003	0.003	0.004
Mg	1.033	0.938	0.914	1.173	0.986	1.059	1.004	1.009
	2.915	2.920	2.877	2.863	2.881	2.933	2.873	2.915
Ca	0.002	0.000	0.001	0.001	0.002	0.004	0.003	0.002
Na	0.045	0.043	0.050	0.040	0.051	0.037	0.036	0.039
K	0.798	0.761	0.793	0.841	0.788	0.761	0.828	0.763
	0.845	0.804	0.844	0.882	0.841	0.802	0.867	0.804
F	0.055	0.046	0.043	0.068	0.043	0.046	0.042	0.045
Cl	0.001	0.003	0.000	0.003	0.004	0.001	0.001	0.003
	0.056	0.049	0.043	0.071	0.047	0.047	0.043	0.048
Fe/Fe+Mg	0.567	0.608	0.609	0.496	0.577	0.564	0.571	0.576

Fe^{3+}, and Ti^{4+} on octahedral sites, and Si^{4+} by Al^{3+} and Fe^{3+} on tetrahedral sites. Replacement of K by Na on the interlayer (XII-fold) site is also common, although in very limited amounts. Substitution mechanisms will be reviewed in the Discussion. Examination of the structural formulas in Table 4 supports the conclusion that biotites deviate from ideal trioctahedral stoichiometry. The deviation ranges from 4.2 to 13.7 percent dioctahedral character.

Biotites from this study have Al^{VI} contents in the range 0.371 to 0.460, consistent with Guidotti's (1984) observation that amphibolite grade biotites have Al^{VI} contents in the range 0.35 to 0.50. These biotites (see Table 4) have 12 to 16% octahedral cations replaced by Al^{VI} and are therefore about 70 to 95 percent of the way toward eastonite-siderophyllite. These results are similar to those obtained by Tracy (1978) and Dymek (1983) for biotites coexisting with phases rich in aluminum, e.g., aluminum silicate or staurolite.

Ti-contents of biotites from The Straits Schist (all coexisting with ilmenite and rutile, see Tables 1 and 4) are comparable to biotites that equilibrated at lower P-T conditions. Kyanite and sillimanite zone biotites in pelites from Mica Creek, British Columbia have higher Ti contents (Stout and others, 1986). Biotites from this study have Ti contents that approach the Ti-content of biotites from Mt. Moosilauke, New Hampshire (Hodges and Spear, 1982), where the P-T conditions approximate those of the Al_2SiO_5 triple point of Holdaway (1971). In general, the Ti content of biotite from The Straits Schist increases as pressure and temperature increase, consistent with results of Engel and Engel (1960), Oki (1961), Kwak (1968), and Guidotti (1984).

Garnet

Table 5 presents microprobe analyses and structural formulas of garnets from the samples examined in this study. Analyses listed in Table 5 were taken just inside the retrograde reaction rim of the garnet. A detailed examination of garnet zoning was not undertaken for purposes of this study, but preliminary results of three garnets indicate that at least two styles or patterns of zoning are present. All the garnets studied show Mn enrichment in the outermost portion of the garnet, possibly due to retrograde equilibration during cooling. Two garnets (TH-16A and CO-5) have zoning patterns similar to each other. Iron and magnesium profiles are complimentary, with Fe increasing and Mg decreasing from core to rim (cf. Figures 4a,b and 5a,b). Manganese shows a profile of enrichment in the core, decreasing from core toward the rim, and then increasing again in the rim region (see Figures 4c and 5c). The Ca profile is similar to the Mn profile in CO-5, but in TH-16A the profile is strikingly different. Calcium begins increasing for a short distance from core to rim, but then begins decreasing until the inner rim, and then increases again (see Figures 4d and 5d). It should be noted here that sample TH-16A contains sillimanite, and CO-5 is from a locality very near fibrolite-bearing rocks.

Profiles of a garnet in sample TH-9 show a different type of zonation. Both Fe and Mg increase from core to rim, but Mg shows a reversal in the rim region (see Figure 6). Both Ca and Mn decrease from core to rim, with Mn showing a reversal (see Figure 6). Sample TH-9 is kyanite-bearing, and has modal garnet greater than modal biotite. A further analysis of garnet zoning will be in the Discussion.

Table 5. Microprobe Analyses of Garnets

	BR-2	CO-1A	CO-5	NH-2A	TH-4	TH-5B	TH-6A	TH-8	TH-9
SiO_2	38.04	38.16	37.19	37.78	37.76	37.21	38.37	37.37	36.87
TiO_2	0.05	0.01	0.02	0.04	0.00	0.03	0.04	0.00	0.00
Al_2O_3	21.65	21.82	21.02	21.98	21.81	21.66	21.67	22.03	21.26
FeO	36.79	37.60	38.12	34.12	37.11	35.46	37.54	33.87	38.06
MnO	0.74	0.68	1.61	3.67	1.25	3.05	1.09	4.39	1.19
MgO	3.41	4.32	3.20	3.04	3.13	3.06	3.29	3.56	3.32
CaO	2.06	0.98	1.18	2.53	2.07	2.12	2.42	1.41	0.93
total	102.74	103.57	102.34	103.16	103.13	102.59	104.42	102.63	101.63
Formulas based on 12 oxygens									
Si	2.981	2.965	2.958	2.956	2.961	2.941	2.972	2.940	2.947
Al	2.000	1.998	1.971	2.027	2.015	2.018	1.978	2.042	2.003
Ti	0.003	0.001	0.001	0.002	0.000	0.002	0.002	0.000	0.000
	2.003	1.999	1.972	2.029	2.015	2.020	1.980	2.042	2.003
Fe	2.411	2.444	2.563	2.233	2.433	2.344	2.432	2.228	2.545
Mn	0.049	0.045	0.108	0.243	0.083	0.204	0.072	0.293	0.081
Mg	0.398	0.500	0.379	0.355	0.366	0.361	0.380	0.417	0.396
Ca	0.173	0.082	0.101	0.212	0.174	0.180	0.201	0.119	0.080
	3.032	3.070	3.125	3.043	3.056	3.088	3.084	3.057	3.100
At % Alm	79.533	79.585	81.164	73.380	79.622	75.899	78.850	72.888	82.070
At % Pyr	13.141	16.300	12.145	11.655	11.971	11.675	12.319	13.657	12.762
At % Sps	1.620	1.458	3.472	7.994	2.716	6.612	2.319	9.568	2.599
At % Gro	5.705	2.657	3.219	6.971	5.690	5.813	6.512	3.887	2.569
Fe/Fe+Mg	0.858	0.830	0.870	0.863	0.869	0.867	0.865	0.842	0.865

Table 5 (continued). Microprobe Analyses of Garnets

	TH-10	TH-13	TH-16A	TH-19	WAT-1A	WAT-3	WAT-4	WAT-5
SiO_2	37.37	36.91	37.09	37.96	37.92	37.34	38.25	37.61
TiO_2	0.00	0.04	0.00	0.05	0.01	0.06	0.07	0.00
Al_2O_3	21.55	21.24	20.88	22.08	21.37	21.16	21.57	21.86
FeO	38.93	38.88	39.08	34.57	37.19	37.88	36.36	35.30
MnO	1.33	1.22	1.90	3.03	1.37	1.05	1.62	1.83
MgO	3.47	3.58	2.87	4.30	3.74	3.40	3.68	3.59
CaO	0.77	0.61	0.64	1.58	1.90	1.90	1.95	1.67
total	103.42	102.48	102.46	103.57	103.50	102.79	103.50	101.86
Formulas based on 12 oxygens								
Si	2.940	2.934	2.960	2.946	2.964	2.951	2.979	2.968
Al	1.998	1.990	1.964	2.020	1.969	1.971	1.980	2.033
Ti	0.000	0.002	0.000	0.003	0.001	0.004	0.004	0.000
	1.998	1.992	1.964	2.023	1.970	1.975	1.984	2.033
Fe	2.562	2.585	2.609	2.244	2.431	2.503	2.368	2.329
Mn	0.089	0.082	0.128	0.199	0.091	0.070	0.107	0.122
Mg	0.407	0.424	0.341	0.498	0.436	0.401	0.427	0.422
Ca	0.065	0.052	0.055	0.131	0.159	0.161	0.163	0.141
	3.122	3.143	3.133	3.072	3.117	3.135	3.065	3.015
At % Alm	82.046	82.235	83.255	73.043	78.001	79.851	77.265	77.256
At % Pyr	13.036	13.498	10.899	16.196	13.983	12.776	13.940	14.006
At % Sps	2.839	2.614	4.100	6.484	2.910	2.242	3.487	4.056
At % Gro	2.079	1.653	1.747	4.277	5.105	5.131	5.309	4.682
Fe/Fe+Mg	0.863	0.859	0.884	0.819	0.848	0.862	0.847	0.847

Figure 4. Compositional zoning maps of a garnet in sample TH-16A.
(a) Fe-zoning map
(b) Mg-zoning map
(c) Mn-zoning map
(d) Ca-zoning map

Sample TH-16A Fe X-Ray Map

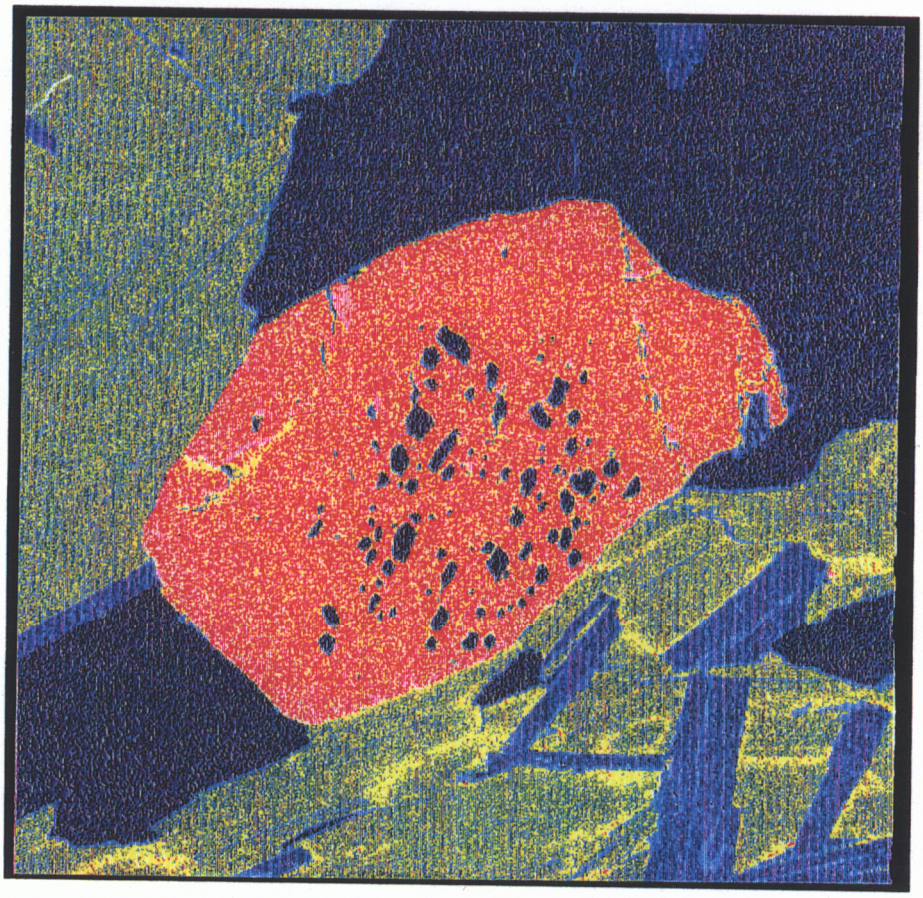

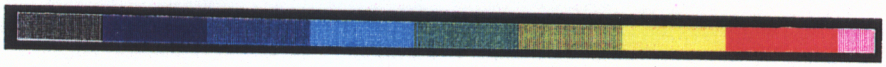

Low ← Relative Count Rates → High

Sampling Resolution: 8μ. Accelerating Potential: 15 keV
Sample current: 200 nA. Data collected on Wavelength Dispersive Spectrometers.

Sample TH-16A Mg X-Ray Map

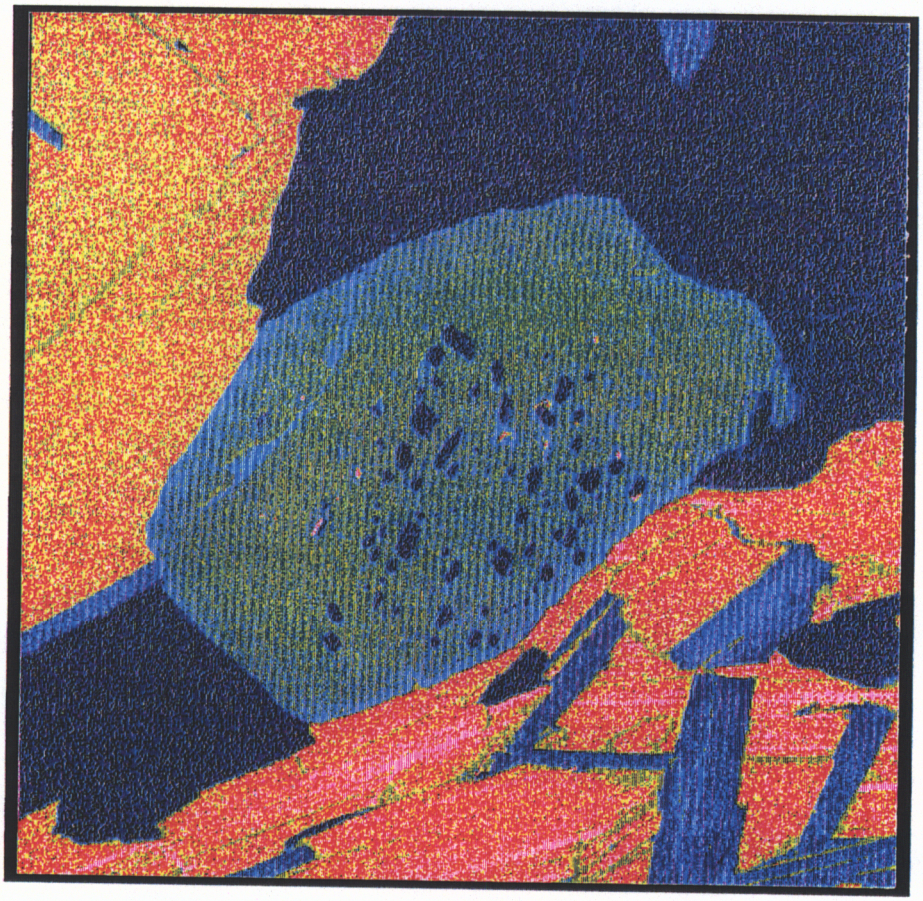

Low ← Relative Count Rates → High

Sampling Resolution: 8μ. Accelerating Potential: 15 keV
Sample current: 200 nA. Data collected on Wavelength Dispersive Spectrometers.

Sample TH-16A Mn X-Ray Map

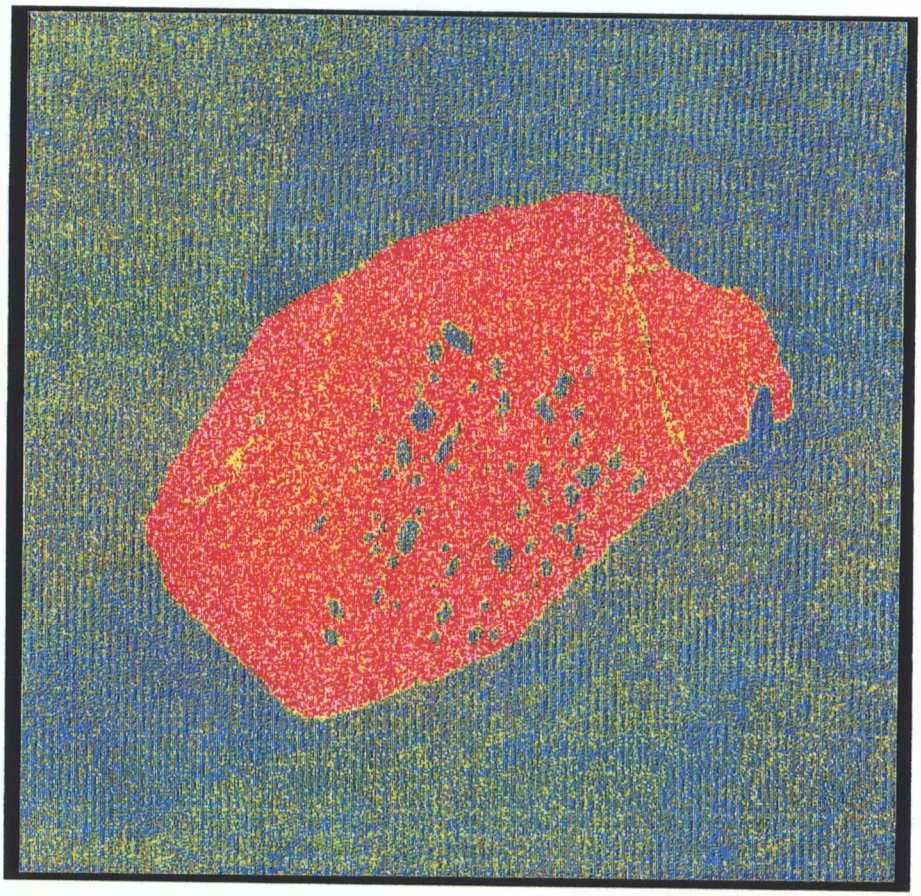

Low ← Relative Count Rates → High

Sampling Resolution: 8μ. Accelerating Potential: 15 keV
Sample current: 200 nA. Data collected on Wavelength Dispersive Spectrometers.

Sample TH-16A Ca X-Ray Map

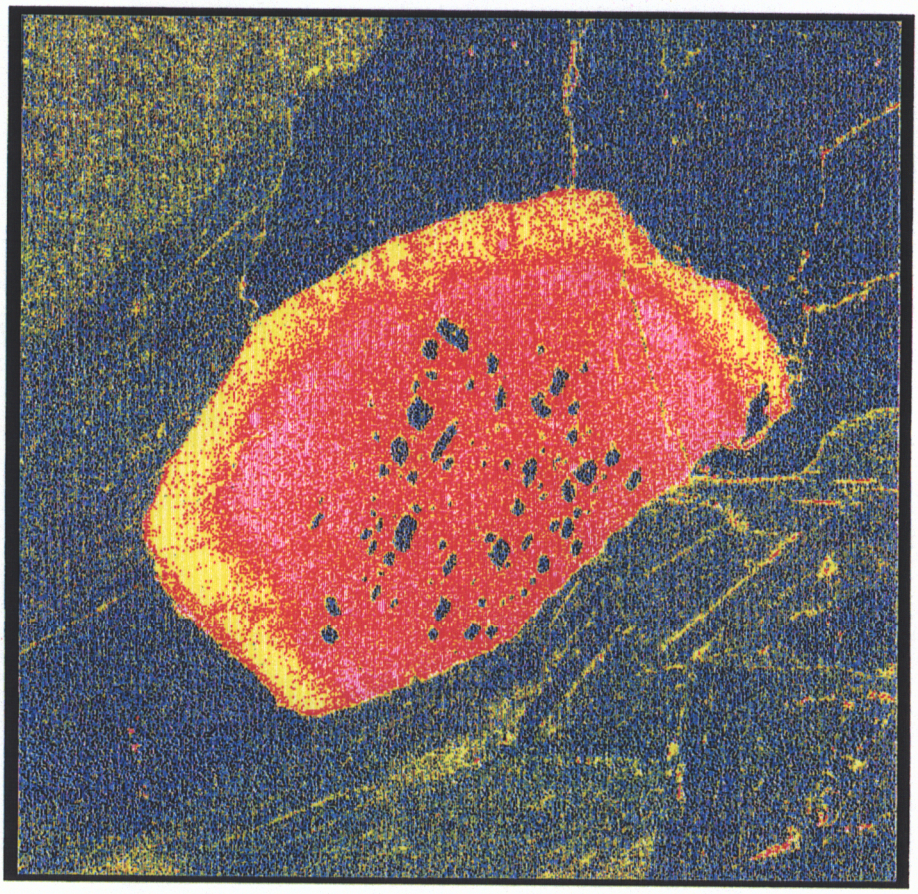

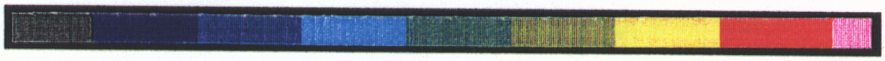

Low ← Relative Count Rates → High

Sampling Resolution: 8μ. Accelerating Potential: 15 keV
Sample current: 200 nA. Data collected on Wavelength Dispersive Spectrometers.

Figure 5. Compositional zoning maps of a garnet in sample CO-5.
(a) Fe-zoning map
(b) Mg-zoning map
(c) Mn-zoning map
(d) Ca-zoning map

Sample CO-5 Fe X-Ray Map

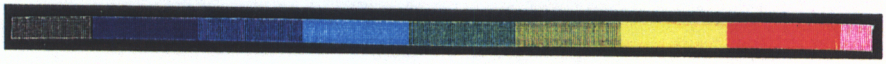

Low ← Relative Count Rates → High

Sampling Resolution: 8μ. Accelerating Potential: 15 keV
Sample current: 200 nA. Data collected on Wavelength Dispersive Spectrometers.

Sample CO-5 Mg X-Ray Map

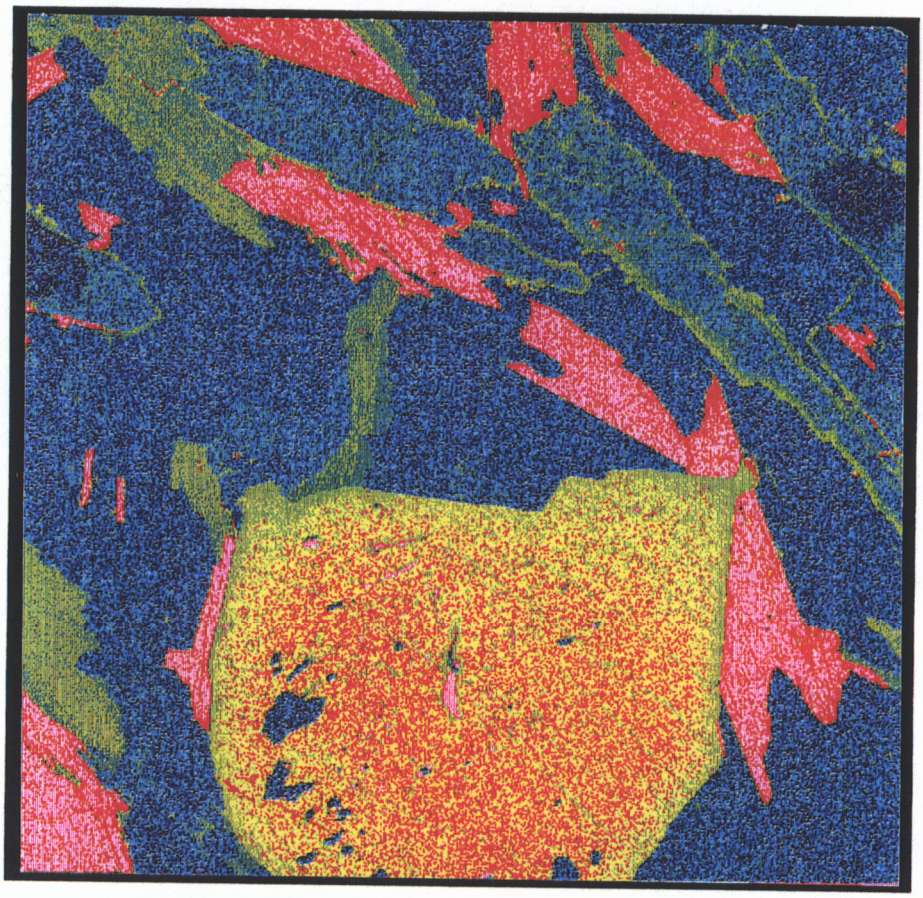

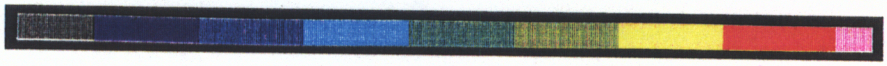

Low ← Relative Count Rates → High

Sampling Resolution: 8μ. Accelerating Potential: 15 keV
Sample current: 200 nA. Data collected on Wavelength Dispersive Spectrometers.

Sample CO-5 Mn X-Ray Map

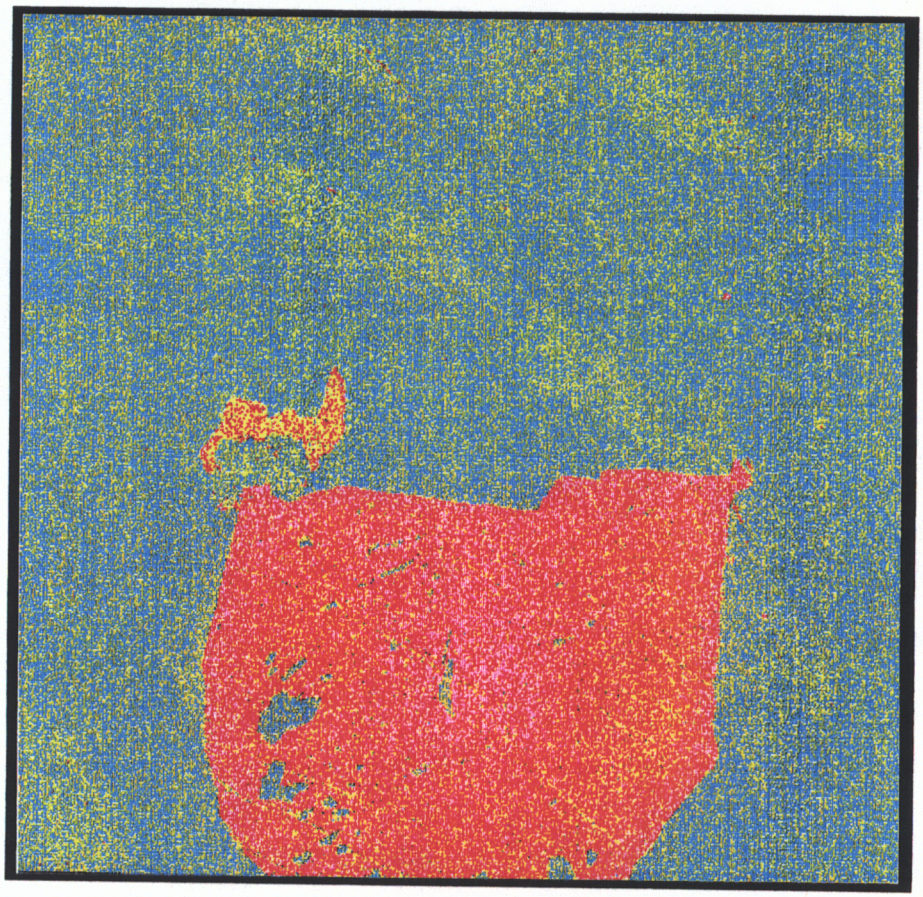

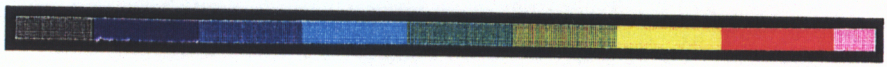

Low ← Relative Count Rates → High

Sampling Resolution: 8μ. Accelerating Potential: 15 keV
Sample current: 200 nA. Data collected on Wavelength Dispersive Spectrometers.

Sample CO-5 Ca X-Ray Map

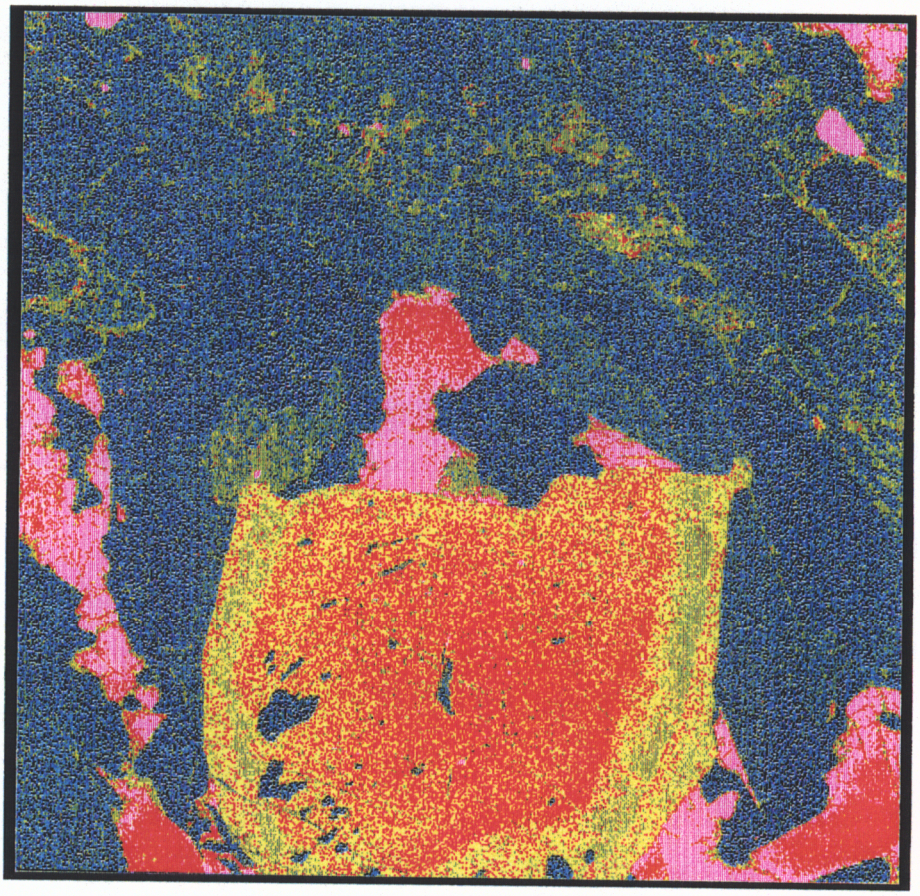

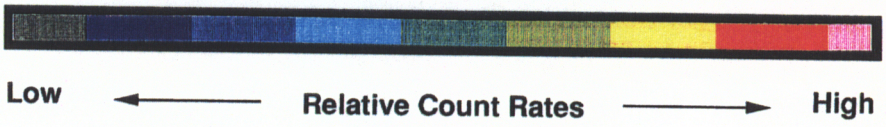

Sampling Resolution: 8μ. Accelerating Potential: 15 keV
Sample current: 200 nA. Data collected on Wavelength Dispersive Spectrometers.

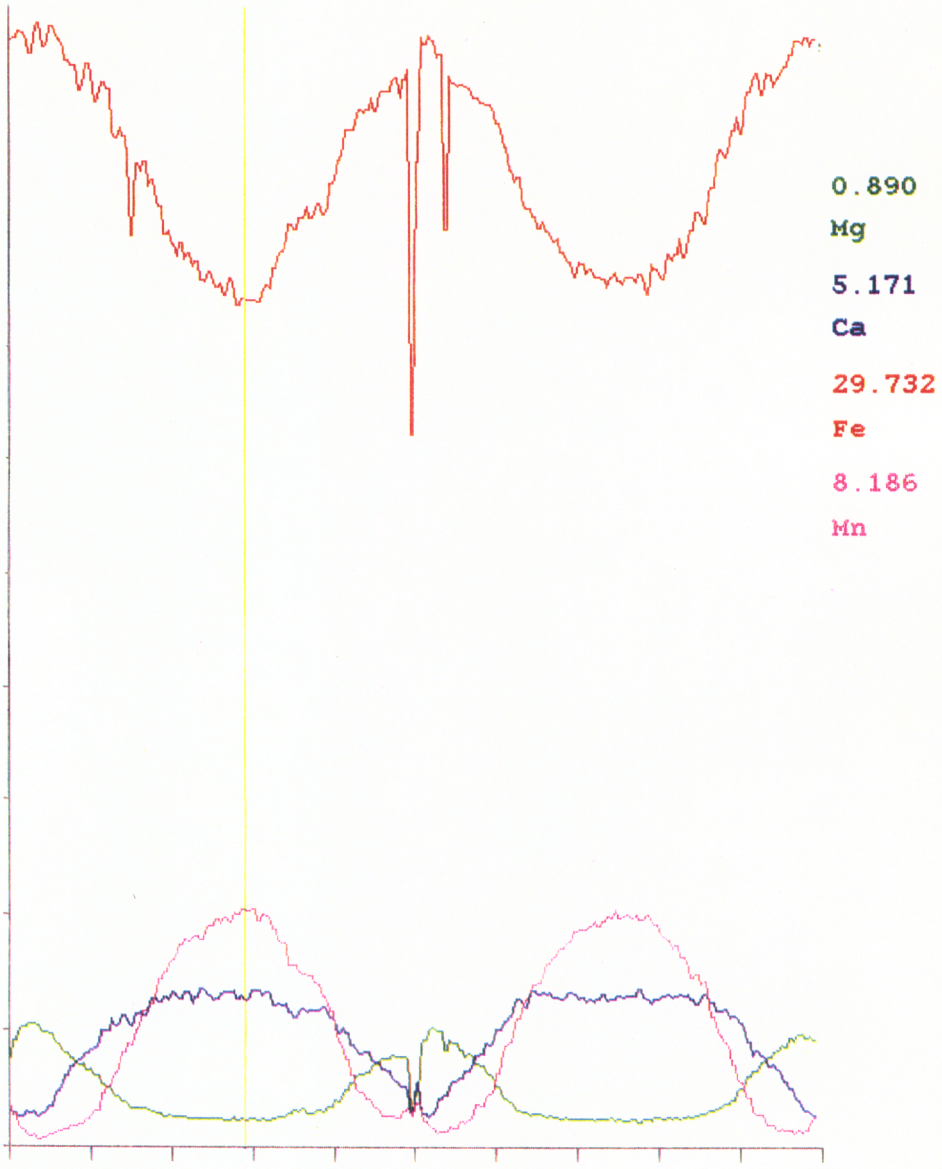

Figure 6. Two compositional profiles perpendicular to each other through the center of a garnet in TH-9.

Figure 7. Compositional zoning profile across a plagioclase–garnet grain boundary in sample CO-5.

Plagioclase

Zoning in plagioclase is not obvious petrographically, but electron microprobe analyses indicate reverse zoning (Ca enriched in rims relative to cores) (see Figure 5d). When plagioclase is in contact with garnet, there is Ca enrichment in the plagioclase and Ca depletion in the adjacent garnet rim. Figure 7 is a profile across a garnet - plagioclase contact from sample CO-5. It should be noted that the $CaAlNa_{-1}Si_{-1}$ interdiffusion is probably at least as slow as cation diffusion in garnets (Yund, 1983), so zoned plagioclase should be as ubiquitous as zoned garnet.

Electron microprobe analyses and structural formulas of plagioclase are given in Table 6. The wide range of plagioclase compositions between samples (approximately An_{13} - An_{29}) probably indicates variations in the bulk composition of the schist, especially variation in Ca/(Ca+Na) (Tracy, 1978).

Ilmenite

Ilmenite is found in all the rocks chosen for electron microprobe study, but not in all the rocks examined (see Table 1). Microprobe analyses of ilmenites from the study area indicate nearly pure $FeTiO_3$, with Mn ranging between 0.35 and 1.25 mol% $MnTiO_3$, and Mg ranging between 0.05 and 0.4 mol% $MgTiO_3$ (see Table 7).

Staurolite

Staurolite is present in trace amounts up to a maximum of 6.6 modal percent in many of the thin sections examined (see Table 1). Table 8 presents microprobe analyses of 11 staurolites from The Straits Schist. The analyses and calculated mineral formulas compare well with other staurolite analyses (Deer, Howie, Zussman, 1962, vol. 1;

Guidotti, 1970; Pigage and Greenwood, 1982). It should be noted here that the ZnO content in staurolites analyzed in this study is quite variable (0.38 to 2.41 wt%). This topic will be discussed further in the Discussion.

Table 6. Microprobe Analyses of Plagioclase

	BR-2	CO-5	NH-2A	TH-4	TH-5B	TH-6A	TH-8
SiO_2	62.76	62.83	61.44	62.85	62.68	61.44	64.29
TiO_2	0.00	0.00	0.00	0.00	0.00	0.00	0.06
Al_2O_3	23.27	23.03	25.00	23.38	23.89	24.76	22.47
FeO	0.10	0.41	0.00	0.00	0.07	0.00	0.05
MgO	0.00	0.00	0.00	0.00	0.00	0.00	0.00
CaO	3.97	4.45	6.10	4.52	4.87	5.71	3.53
Na_2O	9.38	9.08	8.29	9.15	8.93	8.26	9.82
K_2O	0.10	0.08	0.13	0.10	0.09	0.11	0.10
total	99.58	99.88	100.96	100.00	100.53	100.28	100.32
Formulas based on 8 oxygens							
Si	2.787	2.787	2.705	2.781	2.762	2.718	2.829
Al	1.218	1.204	1.297	1.219	1.240	1.291	1.165
	4.005	3.991	4.002	4.000	4.002	4.009	3.994
Ti	0.000	0.000	0.000	0.000	0.000	0.000	0.002
Fe	0.004	0.015	0.000	0.000	0.002	0.000	0.002
Mg	0.000	0.000	0.000	0.000	0.000	0.000	0.000
Ca	0.189	0.212	0.288	0.214	0.230	0.271	0.166
Na	0.808	0.781	0.708	0.785	0.763	0.708	0.838
K	0.006	0.005	0.007	0.006	0.005	0.006	0.006
	1.007	1.013	1.003	1.005	1.000	0.985	1.014
mol % An	18.8	21.2	28.7	21.3	23.0	27.5	16.5
mol % Ab	80.6	78.3	70.6	78.1	76.5	71.9	83.0
mol % Or	0.6	0.5	0.7	0.6	0.5	0.6	0.6

Table 6 (continued). Microprobe Analyses of Plagioclase

	TH-9	TH-10	TH-16A	TH-19	WAT-1A	WAT-4	WAT-5
SiO_2	64.16	64.46	63.69	61.60	63.54	63.65	64.57
TiO_2	0.00	0.00	0.01	0.04	0.01	0.00	0.00
Al_2O_3	22.58	22.23	21.46	23.80	24.24	24.04	23.01
FeO	0.00	0.00	0.01	0.02	0.08	0.08	0.07
MgO	0.00	0.01	0.00	0.02	0.00	0.00	0.01
CaO	3.43	3.24	2.71	4.71	4.63	4.39	3.67
Na_2O	9.89	9.76	10.33	8.78	8.59	8.57	9.46
K_2O	0.04	0.06	0.05	0.11	0.06	0.06	0.08
total	100.10	99.76	98.26	99.08	101.15	100.79	100.87
Formulas based on 8 oxygens							
Si	2.828	2.846	2.858	2.754	2.776	2.784	2.822
Al	1.173	1.157	1.135	1.253	1.235	1.239	1.185
	4.001	4.003	3.993	4.007	4.011	4.023	4.007
Ti	0.000	0.000	0.000	0.001	0.002	0.000	0.000
Fe	0.000	0.000	0.000	0.001	0.006	0.003	0.003
Mg	0.000	0.001	0.000	0.000	0.000	0.000	0.001
Ca	0.162	0.153	0.130	0.226	0.204	0.206	0.172
Na	0.845	0.835	0.899	0.761	0.757	0.727	0.802
K	0.002	0.003	0.003	0.004	0.004	0.003	0.004
	1.009	0.992	1.032	0.995	0.973	0.939	0.982
mol % An	16.0	15.4	12.6	22.7	21.2	22.0	17.6
mol % Ab	83.7	84.2	87.1	76.7	78.4	77.7	82.0
mol % Or	0.2	0.3	0.3	0.6	0.4	0.4	0.5

Table 7. Microprobe Analyses of Ilmenites

	CO-5	TH-5B	TH-8	TH-9	TH-10	TH-16A
SiO_2	0.03	0.04	0.01	0.04	0.02	0.04
TiO_2	52.95	53.16	53.14	53.17	53.67	52.88
Al_2O_3	0.01	0.03	0.01	0.00	0.00	0.00
FeO	48.68	48.06	47.16	48.07	48.21	48.71
MnO	0.67	0.78	1.21	0.94	0.35	0.44
MgO	0.03	0.21	0.12	0.07	0.18	0.13
total	102.37	102.28	101.65	102.29	102.43	102.20

Formulas calculated on the basis of 3 oxygens

Si	0.001	0.001	0.000	0.001	0.000	0.001
Ti	0.987	0.989	0.994	0.990	0.995	0.987
Al	0.000	0.001	0.000	0.000	0.000	0.000
Fe	1.009	0.994	0.981	0.995	0.994	1.011
Mn	0.014	0.016	0.025	0.020	0.007	0.009
Mg	0.001	0.008	0.004	0.003	0.007	0.005
	2.012	2.009	2.004	2.009	2.003	2.013
X_{ilm}*	0.993	0.988	0.986	0.989	0.993	0.993
Fe/Fe+Mg	0.999	0.992	0.995	0.997	0.993	0.995

* X_{ilm} = (Fe+Ti)/(Fe+Ti+Mn+Mg)

Table 8. Microprobe Analyses of Staurolites

	BR-2	CO-1A	CO-5	TH-5B	TH-6A	TH-8
SiO_2	28.42	26.97	27.83	27.16	27.65	27.45
TiO_2	0.69	0.74	0.75	0.53	0.69	0.83
Al_2O_3	53.39	52.36	53.53	53.82	53.05	53.17
FeO	13.33	13.38	12.92	12.49	13.79	13.74
MnO	0.09	0.06	0.07	0.22	0.09	0.31
MgO	1.55	1.41	1.43	1.22	1.42	1.93
ZnO	0.38	2.41	2.38	2.21	0.96	0.98
total	97.85	97.33	98.46	97.65	97.65	98.41

Anhydrous formulas calculated on the basis of 48 oxygens

Si	8.214	7.955	7.952	7.933	8.065	7.961
Al	——	0.045	0.048	0.067	——	0.039
	8.214	8.000	8.000	8.000	8.065	8.000
Al	18.186	18.156	18.275	18.459	18.238	18.136
Ti	0.150	0.164	0.164	0.116	0.151	0.181
Fe	3.222	3.300	3.138	3.051	3.364	3.333
Mn	0.022	0.015	0.017	0.054	0.022	0.076
Mg	0.668	0.620	0.619	0.531	0.617	0.834
Zn	0.081	0.525	0.510	0.477	0.207	0.210
	22.329	22.780	22.723	22.688	22.599	22.770
Fe/Fe+Mg	0.828	0.842	0.835	0.852	0.845	0.800

	TH-9	TH-10	WAT-1A	WAT-4	WAT-5
SiO_2	27.45	27.51	27.71	27.42	27.59
TiO_2	0.73	0.74	0.77	0.75	0.78
Al_2O_3	53.87	53.01	52.28	52.28	54.12
FeO	13.11	14.63	13.45	13.62	13.56
MnO	0.04	0.09	0.12	0.11	0.12
MgO	1.37	1.66	1.55	1.23	1.45
ZnO	1.32	0.98	1.68	1.85	0.94
total	97.89	98.62	97.56	97.26	98.56

Anhydrous formulas calculated on the basis of 48 oxygens

Si	7.974	7.986	8.115	8.071	7.962
Al	0.026	0.014	——	——	0.038
	8.000	8.000	8.115	8.071	8.000
Al	18.416	18.122	18.045	18.136	18.369
Ti	0.159	0.162	0.170	0.166	0.169
Fe	3.185	3.552	3.294	3.353	3.273
Mn	0.010	0.022	0.030	0.027	0.029
Mg	0.593	0.718	0.677	0.540	0.624
Zn	0.283	0.210	0.363	0.402	0.200
	22.646	22.786	22.579	22.624	22.664
Fe/Fe+Mg	0.843	0.832	0.830	0.861	0.840

THERMOBAROMETRY AND FLUID BAROMETRY

Quantitative estimates of the pressure and temperature conditions under which the mineral assemblages of The Straits Schist equilibrated were calculated using calibrated mineral reactions and ion exchange equilibria. Temperatures were calculated using the garnet-biotite exchange equilibria of Thompson (1976) and Ferry and Spear (1978) using the garnet activity models of Hodges and Crowley (1985). Pressures were calculated using the GASP geobarometer of Newton and Haselton (1981) and Koziol and Newton (1988), and the GRAIL geobarometer of Bohlen and others (1983), using the almandine and pyrope activity models of both Bohlen and others (1983) and those of Hodges and Crowley (1985). Pressure and temperature results and ln K_D values are tabulated in Table 9. Calculated temperatures and pressures are also shown on the generalized geologic map in Figures 8 and 9, respectively.

CHOICE OF MINERAL COMPOSITIONS FOR THERMOBAROMETRIC CALCULATIONS

The choice of which measured mineral composition to use in thermobarometric calculations can significantly influence the calculated pressures and temperatures. Quartz, rutile, and the aluminum silicate polymorphs can be treated as stoichiometric thereby making no need for corrections due to impurities or solid solutions. Ilmenite grains of this study show no zonation, therefore an average of ilmenite analyses from single grains will suffice in barometric calculations.

Table 9. Calculated Pressures, Temperatures and ln K_D values

Sample Number	ln K_D§	Temperature* (°C) F&S†	ABT†	Pressure¥ (kbar) GASP	GRAIL[1]	GRAIL[2]	Average[3]
BR-2	1.385	726	720	n.d.**	n.d.	n.d.	n.d.
CO-1A	1.359	738	729	n.d.	n.d.	n.d.	n.d.
CO-5	1.492	679	685	6.6	8.3	8.0	7.4
NH-2A	1.677	607	631	6.9	6.1	5.8	6.4
TH-4	1.586	641	657	7.9	7.7	7.5	7.8
TH-5B	1.630	605	629	6.6	6.8	6.5	6.6
TH-6A	1.545	657	669	7.7	7.7	7.4	7.6
TH-8	1.541	659	670	8.1	6.4	6.1	7.2
TH-9	1.385	726	720	8.0	8.9	8.6	8.4
TH-10	1.536	660	672	6.2	8.4	8.1	7.2
TH-13	1.351	742	732	n.d.	n.d.	n.d.	n.d.
TH-16A	1.567	648	662	6.0	7.9	7.8	6.9
TH-19	1.467	689	693	7.5	6.6	6.1	6.9
WAT-1A	1.346	744	734	9.5	8.0	7.6	8.7
WAT-3	1.518	668	677	n.d.	n.d.	n.d.	n.d.
WAT-4	1.381	727	772	9.3	7.7	7.4	8.4
WAT-5	1.340	747	736	10.3	7.8	7.5	8.9

1 -- GRAIL pressure calculated using the activity model of Bohlen and others(1983)

2 -- GRAIL pressure calculated using the activity models of Hodges and Crowley (1985)

3 -- Average pressure calculated by taking the average of GRAIL[1] and GRAIL[2] and averaging with GASP

* -- Temperatures calculated using the activity models of Hodges and Crowley (1985)

¥ -- Pressures calculated using the temperatures of Ferry and Spear (1978)

** -- n.d. = not determined

§ -- ln K_D calculated on the basis of cations.

K_D of Thompson (1976) = $[(Fe^{gar}Mg^{bio})/(Mg^{gar}Fe^{bio})]$

K of Ferry and Spear (1978) = $(Mg/Fe)_{gar}/(Mg/Fe)_{bio}$

$K = -K_D$

† -- F&S = Ferry and Spear (1978)
ABT = Thompson (1976)

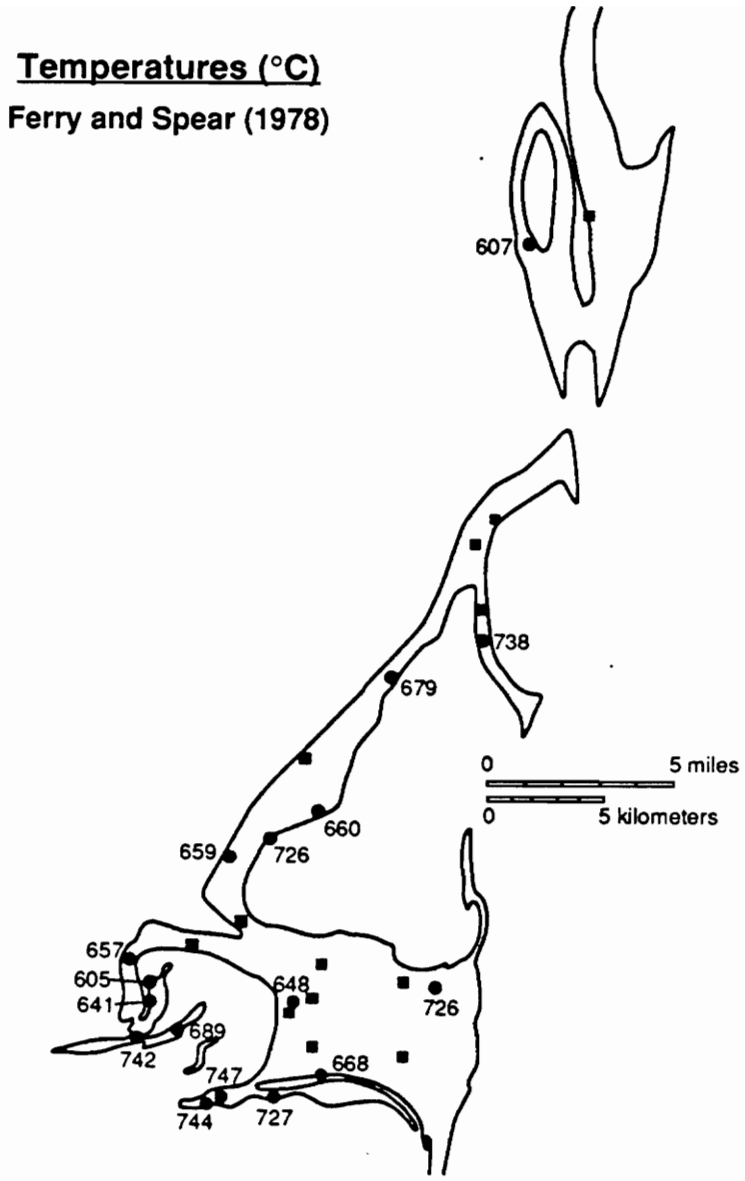

Figure 8. Simplified geologic map showing calculated temperature distribution. Results are presented in degrees C. Solid circles represent samples analyzed by electron microprobe. Solid squares represent samples analyzed petrographically only.

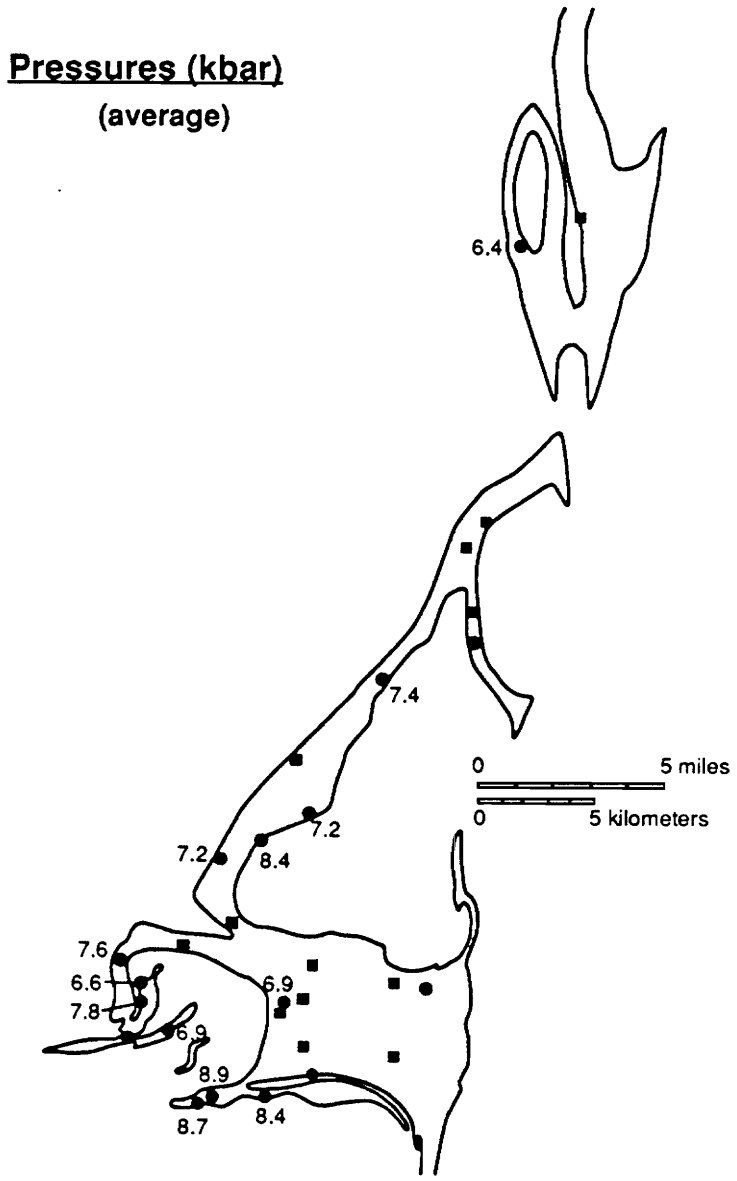

Figure 9. Simplified geologic map showing distribution of calculated pressures. Results are given in kbars. Solid circles represent samples analyzed by electron microprobe. Solid squares represent samples analyzed petrographically only.

Diffusion rates in biotite are typically assumed to be rapid enough to allow homogenization of the grains. However, it is a problem estimating how much the matrix biotite composition might have changed during prograde or retrograde reactions from the composition it had when it was in equilibrium with the garnet composition at peak metamorphic conditions. If modal garnet is much less than modal biotite, it can be assumed that the matrix biotite approached being an infinite reservoir, so the biotite Fe/Mg ratio could not have changed substantially from what it was at peak conditions (Tracy and others, 1976). Therefore, an average of biotite analyses from single grains can generally adequately describe the biotite composition at peak metamorphic conditions. Exceptions to this generalization are found in granulite grade metamorphic rocks, where localized zoning can occur in biotites adjacent to garnet rims (Tracy, 1982).

The choice of garnet and plagioclase compositions, however, can be difficult due to complex zoning. The rims of zoned minerals can (though need not) be strictly in chemical equilibrium with the rest of the rock. Therefore, one must question whether this rim represents peak metamorphic conditions or retrograde cooling conditions.

Composition profiles and X-ray maps of garnet indicate that Mn increases in the rim region (see Figures 4, 5, and 6). If this increase in Mn is due to retrograde cooling effects (Tracy, 1982), then the garnet analysis with the lowest Mn composition is interpreted to be closest to the actual peak metamorphic conditions. This will be the composition used in thermobarometric calculations.

Plagioclase grains exhibit reverse zoning in Ca (see Figures 5d and 7). Since garnet exhibits retrograde cooling effects, it is likely that plagioclase exhibits similar effects. The choice of plagioclase compositions, however, is not as straightforward as that of garnet compositions.

PROBLEMS ASSOCIATED WITH THE P-T ESTIMATES

Inherent in the use of calibrated reactions and exchange equilibria is the fact that the compositions of many natural minerals deviate substantially from the ideal end-member compositions used to calibrate the reactions or that are used in experimental determinations of ion exchange equilibria. Errors may be further complicated and compounded due to mineral compositions falling outside the limits imposed by activity models used in the calibrations (Hodges and McKenna, 1987).

Additional sources of error may be introduced due to incipient alteration of biotites and retrogression of garnet rims. All of the biotites analyzed by electron microprobe in this study show some degree of solid solution toward talc or chlorite based on low (K+Na). This has the effect of forcing biotites toward Mg-richer compositions, thus lowering calculated temperatures and pressures. All the garnets probed show retrograde reaction rims, which also result in the calculated temperatures and pressures being lower than peak metamorphic pressures and temperatures.

TEMPERATURE DETERMINATIONS

Temperatures were calculated from the garnet-biotite Fe-Mg exchange equilibria of Thompson (1976) and Ferry and Spear (1978), using the garnet activity models of Hodges and Crowley (1985). Thompson (1976) calibrated his garnet-biotite geothermometer using natural minerals containing Ca, Mn, Ti, and Al^{VI}. Biotites from The Straits Schist are similar in composition to those used by Thompson (1976). Garnet compositions, however, are substantially different from the garnets used in the Thompson (1976) calibration.

The Ferry and Spear (1978) geothermometer is based on an experimental calibration of the temperature dependence of Fe-Mg partitioning according to the equilibrium:

$$\begin{array}{ccccc} \text{almandine} & + & \text{phlogopite} & & \\ Fe_3Al_2Si_3O_{12} & + & KMg_3AlSi_3O_{10}(OH)_2 & = & \\ Mg_3Al_2Si_3O_{12} & + & KFe_3AlAi_3O_{10}(OH)_2 . & & (1) \\ \text{pyrope} & + & \text{annite} & & \end{array}$$

Their experiments were performed in the absence of Ca and Mn. However, they consider their geothermometer useful up to ≈0.2 (Ca+Mn)/(Ca+Mn+Fe+Mg) in garnet and up to ≈0.15 $(Al^{VI}+Ti)/(Al^{VI}+Ti+Fe+Mg)$ in biotite. Garnets from The Straits Schist do satisfy these compositional constraints. Ferry and Spear's (1978) and Thompson's (1976) K_D values, and thus temperatures, were calculated using the biotite and garnet activity models given in Hodges and Crowley (1985, Table 4).

PRESSURE DETERMINATIONS

Pressures were calculated using the reactions and expressions of Newton and Haselton (1981) (modified by Koziol and Newton, 1988), Bohlen and others (1983), and the almandine activity model of Hodges and Crowley (1985). Newton and Haselton's (1981) GASP (or QGAP) geobarometer is based on the reaction:

$$\begin{array}{ccccc} \text{anorthite} & = & \text{grossular} & + \text{Al-silicate} + \text{quartz} & \\ 3CaAl_2Si_2O_8 & = & Ca_3Al_2Si_3O_{12} & + 2Al_2SiO_5 + SiO_2 . & (2) \end{array}$$

All the rocks in this study chosen for detailed electron microprobe analysis contain the GASP assemblage (see Table 1). Newton and Haselton (1981) stated that solid solution of $Ca_3Al_2Si_3O_{12}$ (grossular) with $Fe_3Al_2Si_3O_{12}$ (almandine) and $Mg_3Al_2Si_3O_{12}$ (pyrope)

lowers the pressure at a given temperature at which the assemblage garnet + Al-silicate + quartz is stable relative to anorthite. Furthermore, solid solution of $CaAl_2Si_2O_8$ (anorthite) with $NaAlSi_3O_8$ (albite) in plagioclase stabilizes plagioclase to higher pressure. Because the concentration of the grossular molecule is typically quite dilute in natural garnets coexisting with plagioclase, an Al_2SiO_5 polymorph, and quartz, the pressure-lowering effect prevails (Newton and Haselton, 1981). The GASP geobarometer is considered valid for garnets low in Mn (Mn $\leq$ 1/3Mg). The Koziol and Newton (1988) redetermination of the end-member anorthite breakdown reaction was the calibration used in this study. Pelites containing the appropriate GASP assemblage have garnet compositions that are typically less than $\approx$5 or so mole% grossular. Garnet analyses may therefore suffer the relatively large errors that can accompany analysis of minor components. Analytical errors may also be compounded by errors resulting from uncertainty in the activity of the grossular molecule at extreme dilution. These errors can be sources of difficulty in the application of the barometer (Bohlen and others, 1983).

The method of Bohlen and others (1983) is useful for rocks containing the assemblage garnet - rutile - Al_2SiO_5 - ilmenite - quartz. This geobarometer (referred to as GRAIL) has been calibrated from the equilibrium relation:

ilmenite + Al-silicate + quartz = almandine + rutile

$$3FeTiO_3 + Al_2SiO_5 + 2SiO_2 = Fe_3Al_2Si_3O_{12} + 3TiO_2 . \qquad (3)$$

This reaction is an especially useful pressure indicator because the end-members involved in the reaction are the dominant constituents of the natural minerals, so the equilibrium conditions for natural rocks are close to those used in the experimental calibration (Yardley, 1989), and the reaction isopleths have shallow P-T slopes lessening error due to

temperature uncertainty (Bohlen and others, 1983). All the rocks in this study chosen for detailed electron microprobe analysis contain the GRAIL assemblage (see Table 1).

Hodges and Crowley's (1985) almandine activity model was also applied to garnets used in the GRAIL geobarometer, and the results are enumerated in Table 9 alongside the pressures calculated using the almandine activity model of Bohlen and others (1983).

CALCULATION OF P_{H_2O}

The partitioning of Na between plagioclase and muscovite can be used to evaluate the variation of intensive parameters (P, T, f_{H_2O}) within rocks from a single, well characterized terrain (Chatterjee and Froese, 1975; Cheney and Guidotti, 1979). The present study employed this Na-partitioning method and calculated pressures and temperatures to estimate f_{H_2O}, and in turn to estimate P_{H_2O} and P_{H_2O}/P_{total}.

Cheney and Guidotti (1979) derived the relationship:

$$\frac{\Delta\mu^{o}}{RT} + \frac{\Delta V_s^{o}}{RT}(P-1) =$$

$$\ln X_{Pg}^{Mu} - \ln X_{Ab}^{Pl} - \ln f_{H_2O} + \ln (X_{Al,M2}^{Mu})^2 +$$

$$\frac{(X_{Mu}^{Mu})^2}{RT}\left[W_{Pg}^{Mu} + 2X_{Pg}^{Mu}(W_{Mu}^{Mu} - W_{Pg}^{Mu})\right]. \qquad (4)$$

Having independent estimates of P and T and using the input parameters listed in Table 10, values of f_{H_2O} can be calculated. Furthermore, calculated intensive parameters are only

relative values due to the uncertainty and arbitrary choice among variables listed in Table 10.

Although f_{H2O} values derived from Equation 4 are relative values, they can be used to place qualitative limits on f_{H2O} within a single metamorphic terrain (Cheney and Guidotti, 1979). Table 11 lists calculated values of f_{H2O}, P_{H2O}, and P_{H2O}/P_{total} across the study area, and Figure 10 is a generalized geologic map with P_{H2O}/P_{total} values shown.

Table 10. Input parameters for Equation (4)

Variable (Eq. 1)	Value	Source	Comments
T	as per Table 9	see text	
P	as per Table 9	see text	
$\ln f_{H2O}$	calculated from equation (1)		
γ_{Ab}^{Pl}	1.0	Orville (1972)	Assumes coupled substitution of $CaAlNa_{-1}Si_{-1}$ with no structural state correction.
$\ln X_{Ab}^{Pl}$	as per Table 6	see text	
$\Delta V_s^o/R$	0.0538 deg/bar	Chaterjee and Froese (1975)	
$\Delta\mu^o/RT$	11,100.71/T-20.47	Chatterjee and Froese (1975) and Holdaway (1971)	The $\Delta\mu^o/T$ term is based on the work of Chatterjee (1972) and corrected to sillimanite on the basis of Holdaway's (1971) results.
$(W_{Pg}^{Mu})/RT$	1,750.95/T+0.0854	Chatterjee and Froese (1975)	
$(W_{Mu}^{Mu})/RT$	2,147.98/T+0.1990	Chatterjee and Froese (1975)	
$(X_{Al,M2})^2$	as per Table 3	see text	Assumes ideal mixing over the M2 site in muscovite

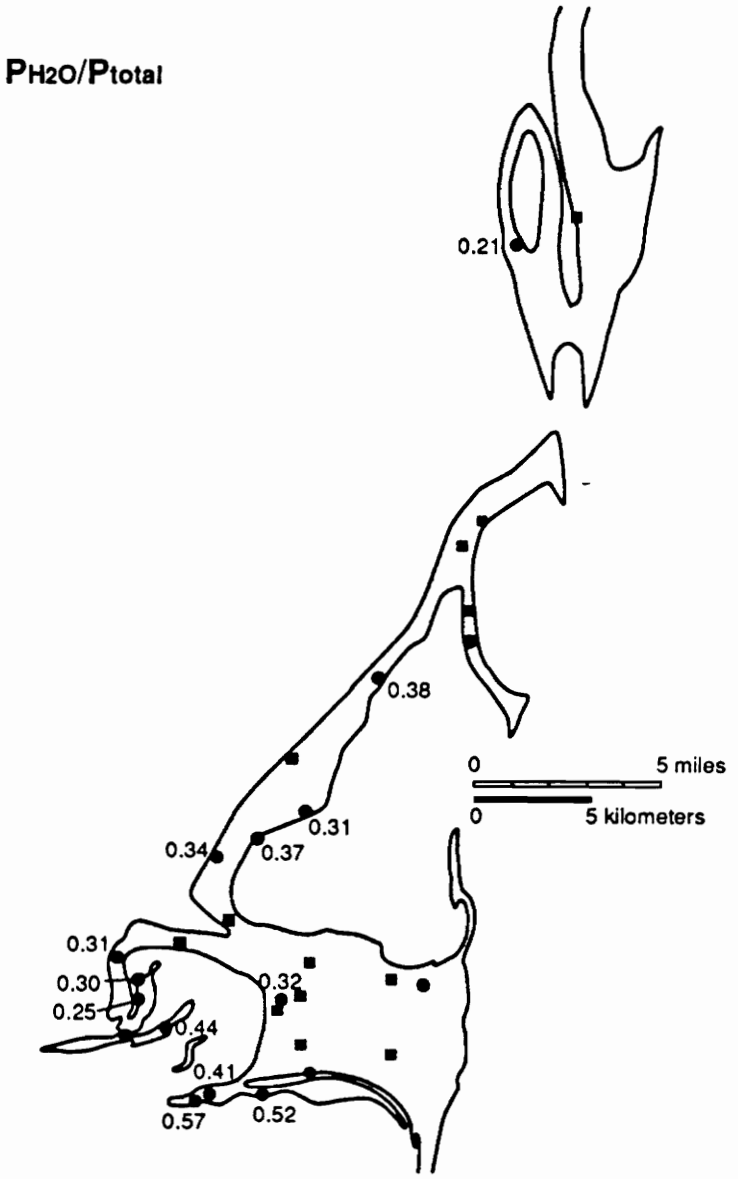

Figure 10. Simplified geologic map showing distribution of P_{H_2O}/P_{total} values. Solid circles represent samples analyzed by electron microprobe. Solid squares represent samples analyzed petrographically only.

Table 11. Calculated values of f_{H_2O}, P_{H_2O}, and P_{H_2O}/P_{total}

Sample	P (bar)	T(°C)	g	f_{H_2O}	P_{H_2O}	P_{H_2O}/P_{total}
CO-5	7400	679	0.9861	2799	2838	0.38
NH-2A	6400	607	0.7342	976	1329	0.21
TH-4	7800	641	0.9663	1866	1931	0.25
TH-5B	6600	624	0.7898	1577	1997	0.30
TH-6A	7600	657	0.9719	2258	2323	0.31
TH-8	7200	659	0.9227	2287	2479	0.34
TH-9	8400	726	1.2156	3824	3146	0.37
TH-10	7200	660	0.9245	2090	2261	0.31
TH-16A	6900	648	0.8582	1870	2179	0.32
TH-19	6900	689	0.9381	2834	3021	0.44
WAT-1A	8700	744	1.2460	5991	4808	0.57
WAT-4	8400	727	1.2160	5305	4363	0.52
WAT-5	8900	747	1.3353	4845	3628	0.41

PHASE EQUILIBRIA

The simplest system in which to represent phase relations of ferromagnesian silicates in metapelites is K_2O - FeO - MgO - MnO - Al_2O_3 - SiO_2 - H_2O (Thompson, 1957). The present phase equilibrium study will be limited to phase compositions that can be shown using the AFM projection from muscovite and quartz of Thompson (1957): biotite, garnet, staurolite, Al_2SiO_5. Examination of the AFM projection (see Figure 11) with the appropriate phases plotted leads to emphasis of two reactions:

kyanite = sillimanite (5)

staurolite + muscovite + quartz =

garnet + biotite + Al_2SiO_5 + H_2O. (6)

KYANITE = SILLIMANITE

The kyanite = sillimanite transition is ideally independent of the activity of H_2O and thus provides general restrictions on the possible pressure - temperature conditions during metamorphism. Because kyanite and sillimanite generally contain only minor impurities, displacement of the kyanite = sillimanite univariant curve is probably negligible (Albee and Chodos, 1969; Chinner, Smith, and Knowles, 1969; Pigage and Greenwood, 1982). For this study, the Holdaway (1971) Al_2SiO_5 triple point was used.

Of the thirty thin sections examined, 19 contain an Al_2SiO_5 polymorph. One thin section (TH-16A) contains prismatic sillimanite, and one thin section (NH-2A) contains

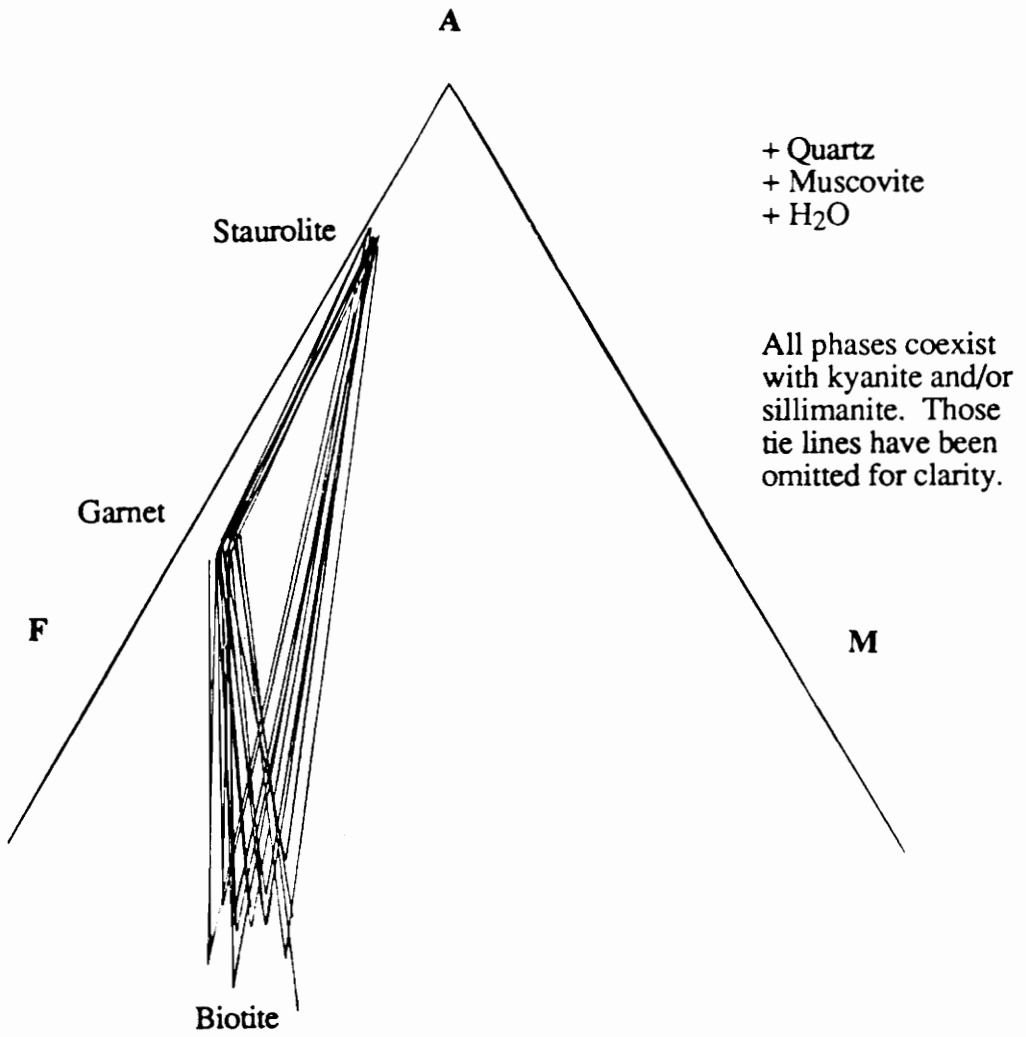

Figure 11. Muscovite AFM projection of garnet, biotite, and staurolite for all samples studied using electron microscopic methods. All phases coexist with kyanite and/or sillimanite (tie lines have been omitted for clarity).

kyanite + fibrolitic sillimanite. The remaining 17 thin sections contain only kyanite (see Table 1).

Kyanite typically persists into the sillimanite stability field due to the fact that the kyanite = sillimanite polymorphic transition is very sluggish (Holdaway, 1971); therefore, any sillimanite found in these rocks is most likely due to the formation of sillimanite from the breakdown of staurolite (Yardley, 1989). Sillimanite may possibly also form from continuous reaction breakdown of the paragonite component of white micas. Having both Al_2SiO_5 polymorphs present indicates that the P-T conditions of The Straits Schist were approximately along the kyanite = sillimanite univariant reaction curve. Pressure and temperature determinations (see Thermobarometry and Fluid Barometry) are consistent with this petrographic observation. Figure 12 is a plot of the Al_2SiO_5 triple invariant point with calculated P-T points plotted, showing the cluster of P-T points around the kyanite = sillimanite univariant reaction curve.

STAUROLITE + MUSCOVITE + QUARTZ = GARNET + BIOTITE + Al-SILICATE + H_2O

Examination of the AFM projection in Figure 11 reveals that one prograde reaction in progress is the terminal discontinuous reaction in the end member system staurolite + muscovite + quartz = garnet + Al_2SiO_5 + biotite + H_2O (reaction (6)). To my knowledge, reaction (6) has not been experimentally calibrated. Hess (1969) did, however, calculate the location on a P-T diagram for the pure Fe-staurolite + muscovite reaction (see Figure 13). The observation that staurolite apparently does not commonly coexist with K-spar, and therefore the staurolite field must disappear in a P-T region within the stability field of muscovite + quartz (Hess, 1969), is consistent with petrographic observations of The

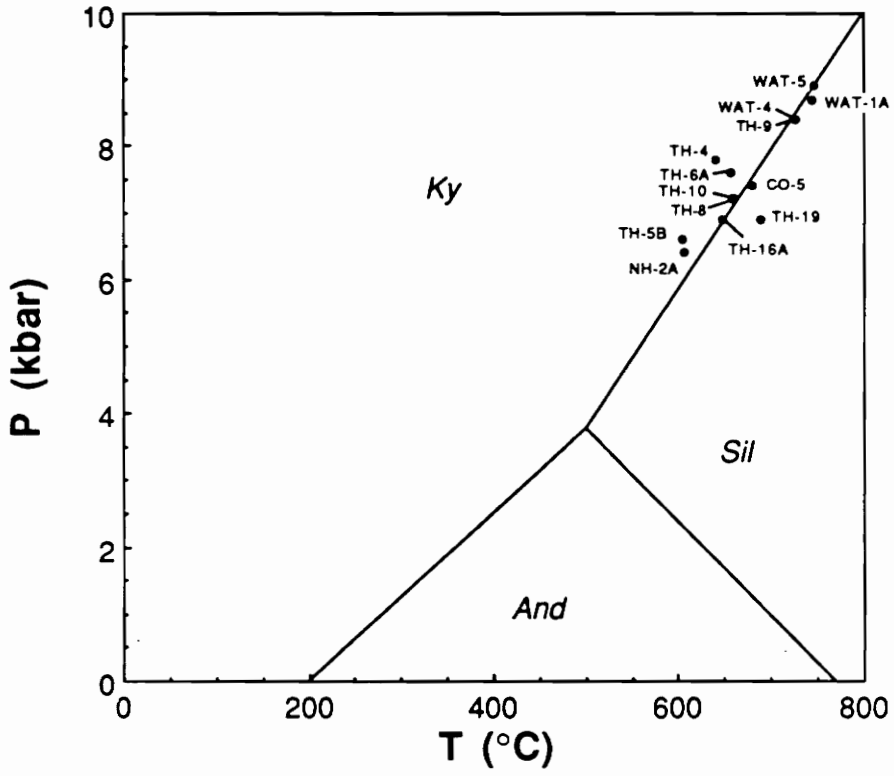

Figure 12. Pressure-temperature plot of calculated thermobarometric results overlain on the Al_2SiO_5 triple point of Holdaway (1971).

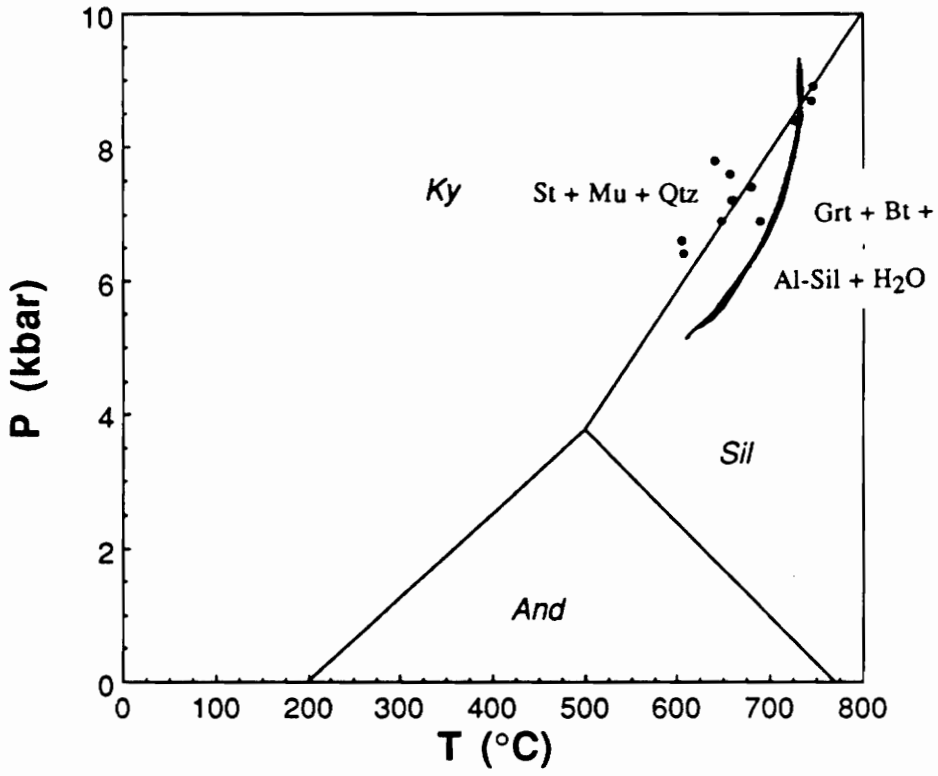

Figure 13. Pressure-temperature plot of calculated thermobarometric results overlain on the Al_2SiO_5 triple point of Holdaway (1971). Also shown is the staurolite + muscovite breakdown reaction calculated by Hess (1969).

Straits Schist. Thompson (1976) went further in locating reaction (6) in P-T space by determining that at 5 kbar, reaction (6) lies at higher temperatures than the reaction

$$\text{staurolite} + \text{quartz} = Al_2SiO_5 + \text{garnet} + H_2O\,, \qquad (7)$$

and at lower temperatures than the reaction

$$\text{muscovite} + \text{quartz} = \text{K-feldspar} + \text{sillimanite} + H_2O\,. \qquad (8)$$

Assuming Hess's (1969) calculated calibration for the end members is reasonably correct, and that Thompson's (1976) location between the staurolite + quartz and muscovite + quartz breakdown reactions is correct, extrapolation to ≈7.5 kbar yields a reaction temperature of approximately 710°C. This result is entirely consistent with calculated pressures and temperatures (see Thermobarometry and Fluid Barometry).

DISCUSSION

IMPLICATIONS OF GARNET ZONING

Generally, zoning patterns of kyanite-staurolite-grade garnets show an increase in Fe and Mg as Mn and Ca decrease from core to rim and Mg commonly shows a reversal in zoning near the rim (Tracy, 1982). Comparison of x-ray maps and profiles of several garnets from The Straits Schist reveal zoning patterns that are strikingly different from each other (cf. Figures 4, 5, and 6). One garnet (from TH-9) has a zoning pattern similar to typical kyanite-staurolite-grade garnets, the difference being that TH-9 shows reversals in Mg, Ca, and Mn (see Figure 6). This garnet exhibits roughly concentric normal chemical zoning (Hollister, 1966). It also shows a trend toward lower Mn, but very little change in Mg/Fe from core to rim. This cannot be explained by a continuous Fe-Mg reaction, but may be due to the effects of Mn on the terminal discontinuous Fe-Mg reaction

$$\text{staurolite} + \text{muscovite} + \text{quartz} = \text{Al-silicate} + \text{garnet} + \text{biotite} + H_2O \qquad (6)$$

which can be thought of as a continuous Fe-Mg-Mn reaction with $T_{Fe} \geq T_{Mg} > T_{Mn}$ (Tracy and others, 1976). The change in zoning toward lower Mg and higher Mn and Ca in the outermost rim region may be due to other prograde continuous reactions or to retrograde cooling reactions.

Zoning in garnets from samples TH-16A and CO-5 is different from garnet zoning in TH-9 (compare Figures 4, 5, and 6). Garnets from TH-16A and CO-5 show a core-to-rim decrease in Mn, with a rim reversal, similar to TH-9. Unlike TH-9, however, TH-16A

and CO-5 show a continuous increase in the Fe/Mg ratio from core to rim. Calcium shows a more complex zoning pattern. The sense of zoning of Mg in TH-16A and CO-5 is the opposite of that in TH-9. Therefore, the zoning trends toward higher Fe/Mg in TH-16A and CO-5. Reaction (6) was used to explain garnet zoning in TH-9 due to the effects of Mn on the reaction. Reaction (6) could also explain zoning in TH-16A and CO-5 if the effects of Mn were negligible in these particular samples (e.g., perhaps the bulk composition might be slightly deficient in Mn compared to TH-9). As reaction (6) progressed, staurolite was consumed, releasing Fe and therefore making more Fe available for incorporation into garnet and biotite structures.

Calcium zoning in the rim could be due to retrograde reequilibration during cooling. The analyzed garnet in sample TH-16A has an unusual Ca-zoning profile. Calcium initially begins to increase in the core region, and then begins decreasing. Perhaps at this stage of garnet growth, a calcic phase was involved that produced this particular zoning profile which just happened to be preserved in this garnet but was not preserved, or never existed, in other garnets.

OTHER MINERALS

Muscovites, biotites, and other phases are chemically complex; therefore, there are numerous sets of linearly independent exchange components with which to describe the composition of a naturally occurring crystal (Hewitt and Abrecht, 1986). Although it has been generally accepted that incomplete analyses will lead to ambiguous results regarding substitutions, it can also be demonstrated that even with complete mineral analyses it is not possible to make unique substitution models (Hewitt and Abrecht, 1986). With this in

mind, the following is a brief discussion of the substitutions that may be of importance in the muscovites and biotites from The Straits Schist.

Deviations of muscovite from ideal white mica stoichiometry can be accomplished through one or more simple or coupled, single- or multi-site substitutions in the crystal structure. One substitution is the Tschermak substitution, which involves both octahedral and tetrahedral sites:

$$(Al^{3+})^{VI} + (Al^{3+})^{IV} = (R^{2+})^{VI} + (Si^{4+})^{IV}. \quad (9)$$

If $(R^{2+})^{VI}$ and $[(Si^{4+})^{IV} > 3.0]$ in muscovite were due only to substitution (9), a plot of $(Si^{4+})^{IV}$ *versus* $(R^{2+})^{VI}$ should produce a line connecting ideal muscovite and ideal phengite that has a slope of 1.00. The plot of $(Si^{4+})^{IV}$ *versus* $(R^{2+})^{VI}$ in Figure 14 shows that the data plot above the ideal Tschermak line, and a best-fit line to the data has a slope of approximately 0.86. An exchange such as:

$$2(Al^{3+})^{VI} = (Ti^{4+})^{VI} + (R^{2+})^{VI} \quad (10)$$

might explain the fact that the data points on Figure 14 fall on a line which lies above the ideal Tschermak line (Guidotti, 1984).

Additional deviation might be due to the substitution:

$$(Fe^{3+})^{VI} = (Al^{3+})^{VI}. \quad (11)$$

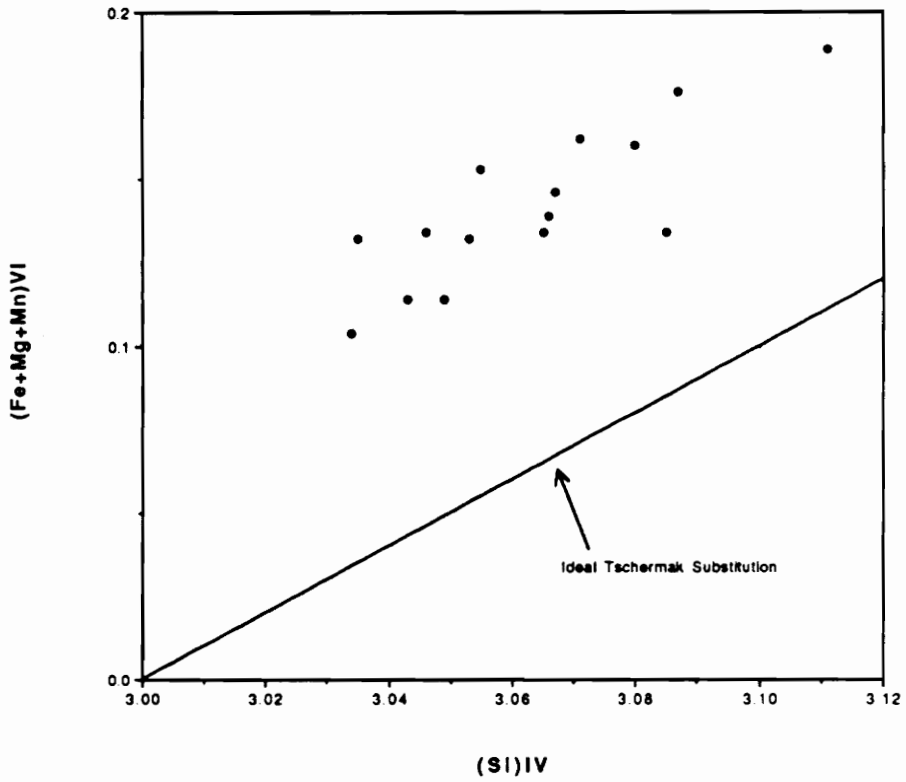

Figure 14. $(Fe^{2+}+Mg+Mn)^{VI}$ *versus* $(Si)^{IV}$ in muscovite. Notice that all points plotted lie above the Ideal Tschermak Substitution line (see Text for discussion).

This would have the effect of removing Fe^{3+} from Fe^{tot}, thus lowering the sum of Fe^{tot} + Mg + Mn, which will result in the moving of data points on Figure 14 closer to the ideal Tschermak substitution.

Replacement of octahedral Al by Fe^{2+}, Mg, Mn, and Ti and the replacement of tetrahedral Al by Si are the only two substitutions which are quantitatively important (Tracy, 1978). These two substitutions can be combined to enable a graphical evaluation of the extent to which these substitutions have taken place (Tracy, 1978; Dietsch, 1988):

$$(Fe^{2+}+Mg+Mn+Ti^{4+})^{VI} + (Si-3.0)^{IV} = (2.0-Al)^{VI} + (1.0-Al)^{IV}. \qquad (12)$$

Figure 15 is a plot of both dioctahedral and trioctahedral compositional trends and the actual compositions of analyzed muscovite and biotite from The Straits Schist. Examination of Figure 15 shows that the white micas are very close to ideal dioctahedral stoichiometry, however they do deviate somewhat towards a trioctahedral composition.

As has already been mentioned above (see Petrography and Mineral Chemistry — Muscovite), muscovites from The Straits Schist are Na-rich (≈12 to 20 mol% Na). Muscovites from a lower-pressure terrain in central Massachusetts which were at or near temperatures of the muscovite breakdown reaction to sillimanite + K-feldspar have paragonite contents that range between 0.67 and 5.8 mol% (Tracy, 1978; Cheney and Guidotti, 1979). Results of this study indicate that muscovites from The Straits Schist are more Na-rich than muscovites from pelitic schists of lower grade terrains. Examination of Figure 16 reveals that, in general, muscovites from The Straits Schist are at higher calculated P-T conditions are indeed more Na-rich than muscovites at lower calculated P-T conditions. Whereas this relationship is not always the case, the higher Na-contents of

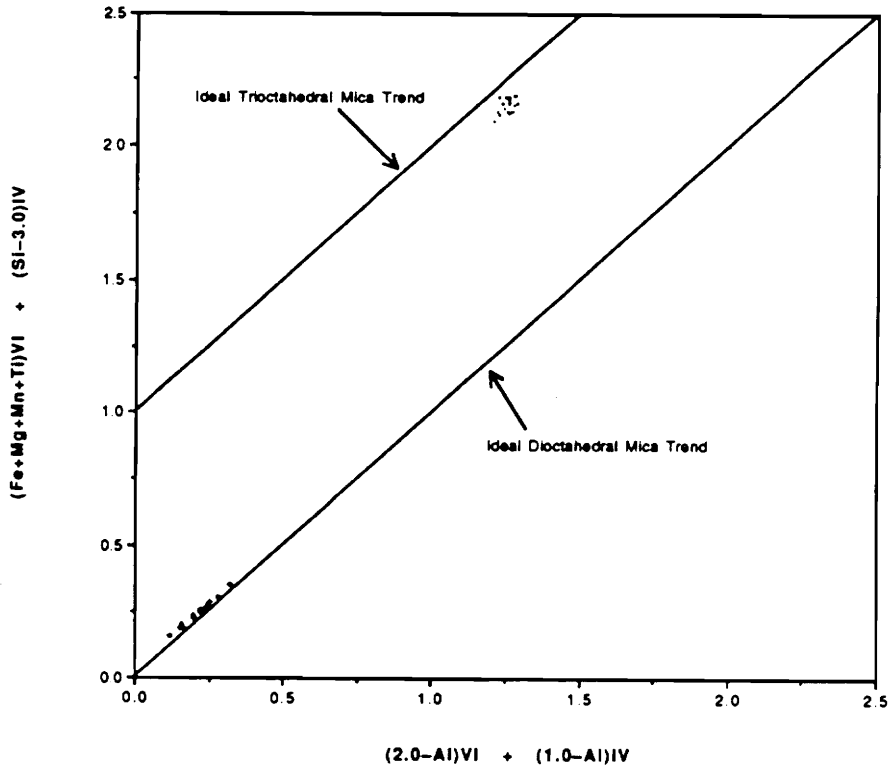

Figure 15. Plot of mica compositions combining the substitutions of Al by Fe, Mg, Mn, and Ti in octahedral sites and Si by Al in tetrahedral sites, after Tracy (1978). Fe is shown as Fe^{total}. Also shown are ideal dioctahedral and trioctahedral mica trends.

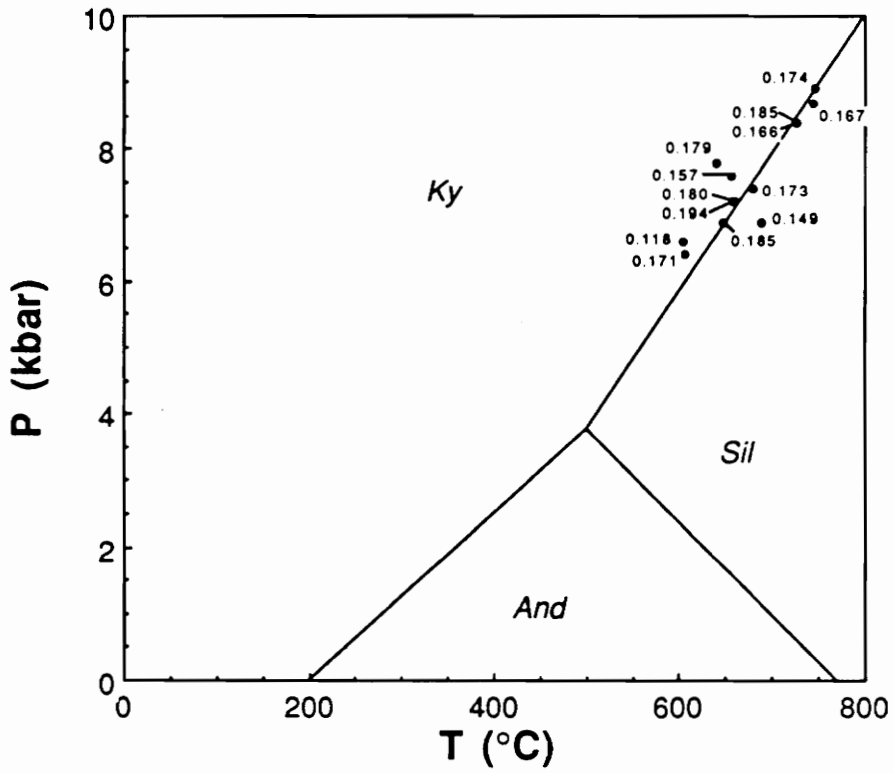

Figure 16. Pressure–temperature plot showing Na/(Na+K) values for muscovite.

muscovites that are at somewhat lower P-T conditions could be due to the calculated pressures and temperatures being retrograde rather than peak metamorphic conditions.

As in muscovite, deviation of biotite within and from the ideal four biotite end-member stoichiometry can be accomplished through one or more simple or coupled, single- or multi-site substitutions. Biotite crystal chemistry can be complicated by the occurrence of vacancies. Foster (1960a,b) demonstrated that octahedral occupancy in biotite is generally less than three cations/formula. Recalculated biotite interlayer site occupancies are virtually always less than one.

The main mechanism causing Al-enrichment in biotite may be the Al-Tschermak's substitution:

$$(R^{2+})^{VI} + (Si^{4+})^{IV} = (Al^{3+})^{VI} + Al(^{3+})^{IV}\,, \qquad (13)$$

which relates phlogopite-annite to eastonite-siderophyllite. The amount of Al-Tschermak substitution increases slightly up to sillimanite grade, and may even decrease at higher grades (Tracy and Robinson, 1978; Dymek, 1983).

Many biotites contain Al^{VI} that can not be explained by substitution (6) (Foster, 1960a,b; Dymek, 1983). Additional Al can be incorporated through a dioctahedral-trioctahedral substitution:

$$3(R^{2+})^{VI} = 2(Al^{3+})^{VI} + [\ ]^{VI}, \qquad (14)$$

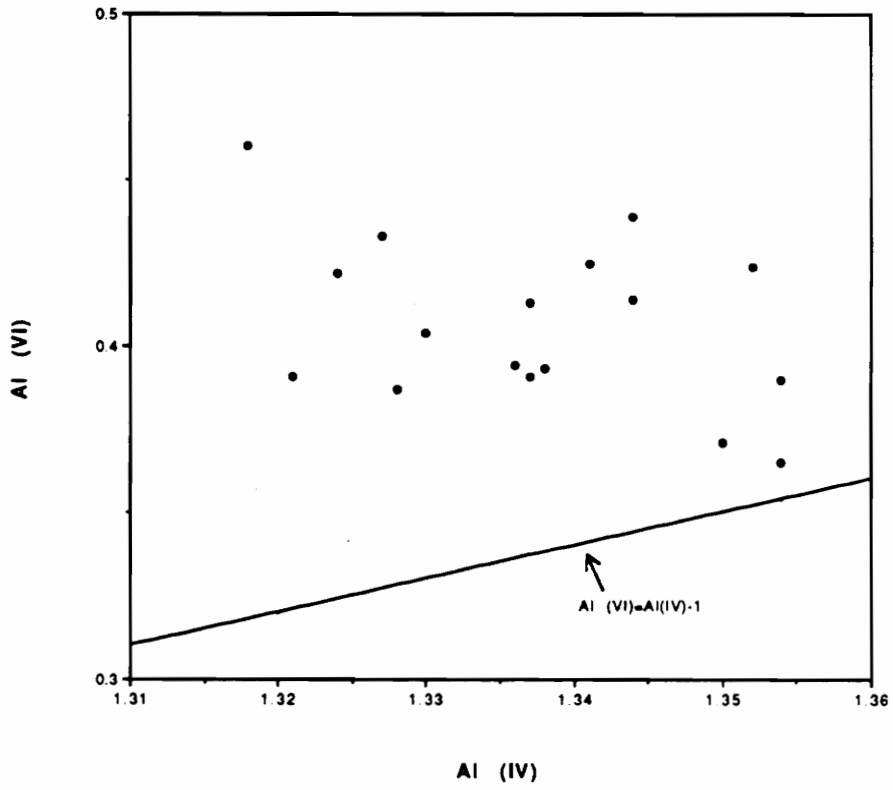

Figure 17. Plot of Al^{VI} *versus* Al^{IV} in biotite. Notice that all points plot above the $Al^{VI}=Al^{IV}-1$ line. See Text for discussion.

which can be considered a muscovite component in biotite, resulting in the formation of vacancies. Observations on natural biotites suggest that substitution (14) is maximized in biotite coexisting with muscovite (Dymek, 1983).

If the substitution of Al^{VI} into biotite occurred only by the Al-Tschermak's component (13), then data points should fall along the line labeled Al(VI) = [Al(IV)-1] shown in Figure 17 (Dymek, 1983). The effect of substitution (11) should result in Al^{VI} exceeding Al^{IV} in direct proportion to the amount of $(Fe^{3+})^{VI}$. All biotites in this study plot above the Al(VI) = [Al(IV)–1] line (see Figure 17), indicating Al^{VI} not balanced by Al^{IV}. These results are entirely consistent with the interpretation that there is a ferric iron component to these biotites.

If the dioctahedral-trioctahedral substitution (14) were operating, data should plot along a line proportional to $3/2Al^{VI}$ on a plot of Total Positive Charge *versus* Al^{VI}. As can be seen in Figure 18, no such correlation exists, indicating that substitution (14) may not play a significant role.

Although Ti substitution in biotite has been investigated by many workers (e.g., Bohlen and others, 1980; Guidotti and others, 1977; Labotka, 1983; Abrecht and Hewitt, 1986), there is still no consensus as to the nature of Ti substitution in biotite. It is widely accepted that Ti occurs as $(Ti^{4+})^{VI}$, and this convention will be followed here. It is known that Ti content in biotite is maximized in the case of biotite coexisting with a Ti-rich phase (ilmenite or rutile), ensuring that the biotite is saturated with Ti and thus making the Ti content only a function of intensive parameters (Guidotti, 1984). Several substitutions have been suggested for Ti^{4+} in biotite (see for example Dymek, 1983; Guidotti, 1984; Abrecht and Hewitt, 1986). Evidence presented here (below) and results of other investigators suggest that there are two dominant Ti substitutions in biotite (Tracy, 1978;

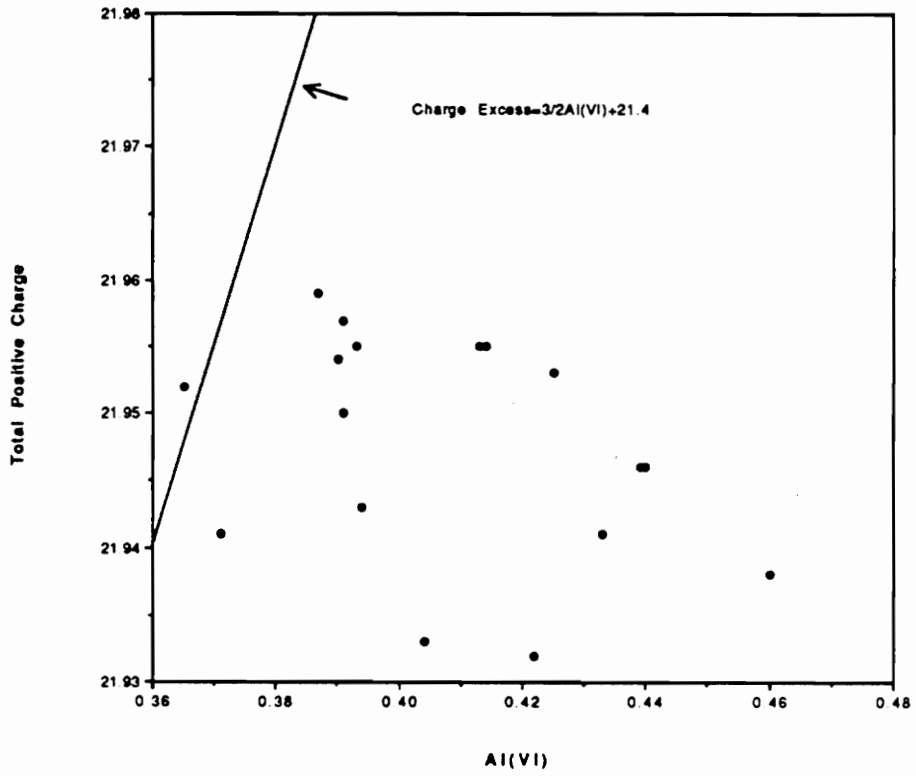

Figure 18. Plot of Total Positive Charge *versus* Al^{VI} in biotite. See Text for discussion.

Dymek, 1983; Guidotti, 1984; Abrecht and Hewitt, 1986). The first involves the Ti-Tschermak's component, a VI- and IV-fold coupled substitution:

$$(R^{2+})^{VI} + 2(Si^{4+})^{IV} = (Ti^{4+})^{VI} + 2(Al^{3+})^{IV}. \quad (15)$$

The second involves only octahedral sites:

$$2(R^{2+})^{VI} = (Ti^{4+})^{VI} + [\ ]^{VI}. \quad (16)$$

Substitution (16) results in the formation of octahedral vacancies.

As in the case of muscovite, ferric iron may be incorporated via substitution (4). This substitution should be maximized when biotite coexists with a Fe^{3+}-saturating phase such as magnetite or hematite. Distinction between Fe from substitution (11) and Fe from substitutions (13), (14), (15), and (16) requires distinguishing between Fe^{2+} and Fe^{3+}, which is not possible using the electron microprobe (Guidotti, 1984). Arguments have been made to attempt to qualitatively confirm the presence or absence of Fe^{3+}. It is generally accepted that rocks containing graphite and ilmenite are reduced and will therefore have mostly reduced Fe (Tracy, 1978; Guidotti, 1984; Dietsch, 1988). However, recent results from Dyar (1990) using Mössbauer spectroscopy indicate that even in reduced pelitic rocks, biotites contain between 1.0 and 2.7 wt% Fe_2O_3. This leads to the conclusion that these biotites may in fact contain Fe^{3+}, which could explain some of the deviation from ideal annite-phlogopite stoichiometry.

Substitutions involving the XII-fold (interlayer) sites may arise from two sources. Substitution of H_3O^+ for K^+ could explain the interlayer site deficiencies found in biotite recalculations from electron microprobe analyses (Dymek, 1983). Interlayer site

deficiencies may also be due to the substitution relating phlogopite-annite to a talc component (Dymek, 1983):

$$(K^{+})^{XII} + (Al^{3+})^{IV} = [\ ]^{XII} + (Si^{4+})^{IV}. \qquad (17)$$

Furthermore, the K-Na substitution relates phlogopite to its Na-counterpart wonesite, and it also relates eastonite to preiswerkite.

If all Ti^{VI} and Al^{IV} were balanced by substitution (15), then data points on a Ti^{VI} vs. Al^{IV} plot should lie on the line labeled Ti/[Al(IV)–1] = 1/2. Data falling below this line could be interpreted as resulting from the combined effects of the Al- and Ti-Tschermak's substitutions [(13) and (15)] (Dymek, 1983). As can be seen on Figure 19, all the data plot below the Ti/[Al(IV)-1] = 1/2 line. Dymek (1983) stated that this is a necessary but not sufficient condition for supporting the above interpretation, supporting the conclusion that substitutions (13) and (15) may be operating.

Figure 20 shows the relationship between calculated positive charge and Ti-content. The line labeled Charge Excess = 2Ti is not constructed to fit the data. Rather, it is a line drawn from zero Ti-content and total positive charge equal to twenty-two, with a slope of two. A correlation between charge excess and Ti-content suggests that substitution (15) plays a minor role for Ti-substitutions, and that the Ti-vacancy (16) substitution may be operating (Dymek, 1983). A lack of correlation, as is the case here, is interpreted to indicate that substitution (15) may play a significant role. The total positive charge used in Figure 18 is calculated assuming all iron if Fe^{2+}. If some of the iron is Fe^{3+}, then the total positive charge is higher and the charge excess (the difference between the values along the line Charge Excess = 2Ti and the calculated total positive charge) is lower. The result of

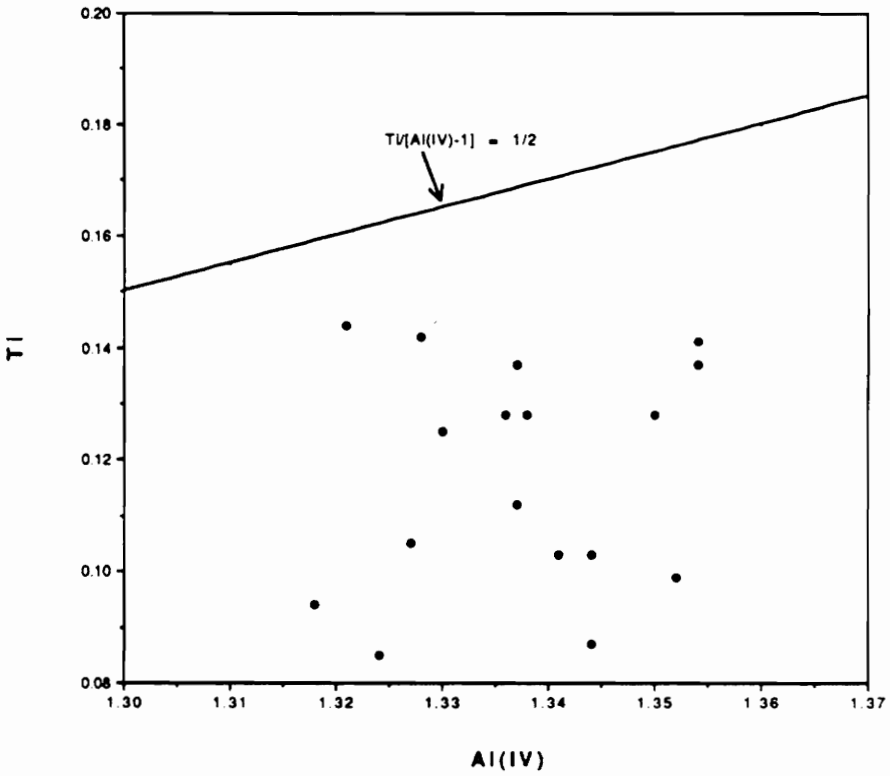

Figure 19. Plot of Ti *versus* Al^{IV} in biotite. Notice that all points plot below the Ti/[Al^{IV}–1] line. See Text for discussion.

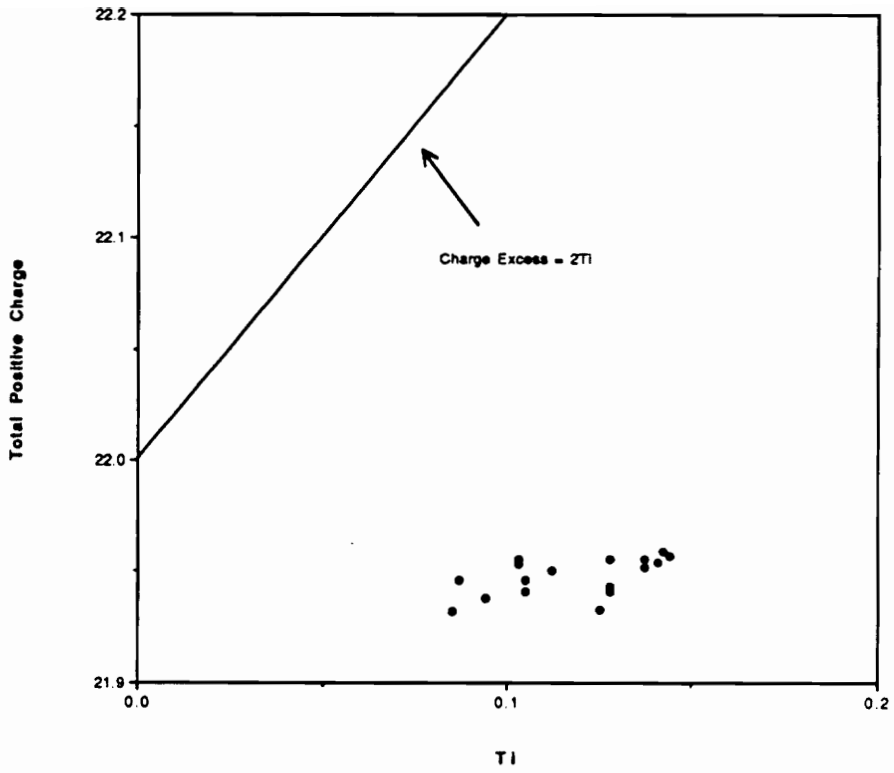

Figure 20. Plot of Total Positive Charge *versus* Ti in biotite. Notice that all points plot below the Charge Excess = 2Ti line. See Text for discussion.

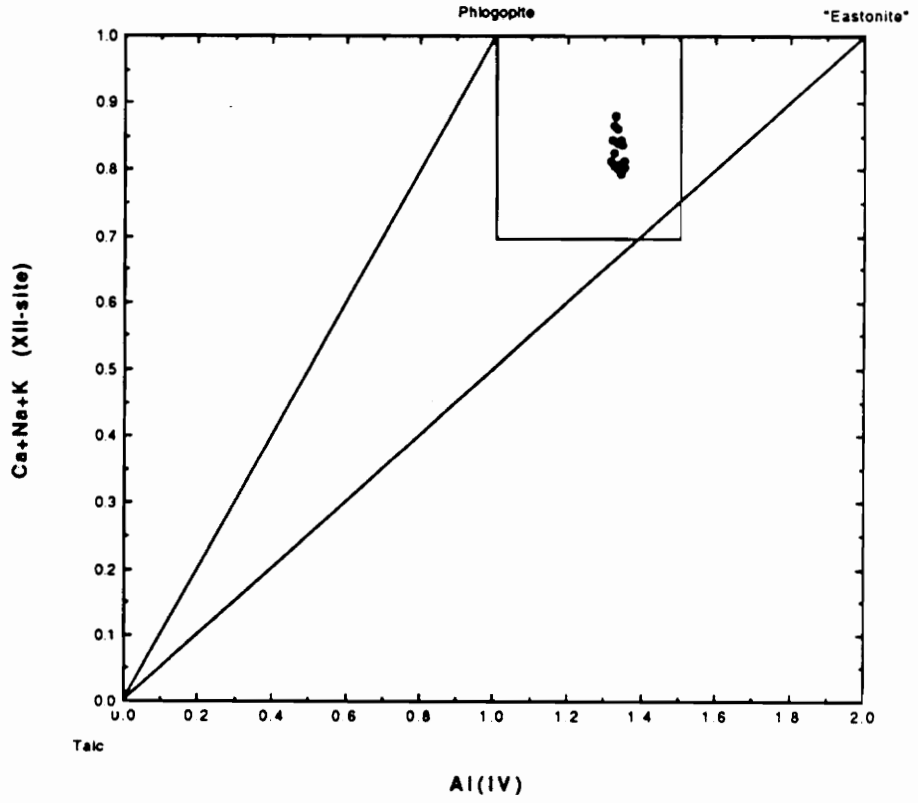

Figure 21. $(Ca+Na+K)^{XII}$ variation diagram illustrating the substitutional relationships among talc, phlogopite, and "eastonite." See Text for discussion. After Dymek (1983).

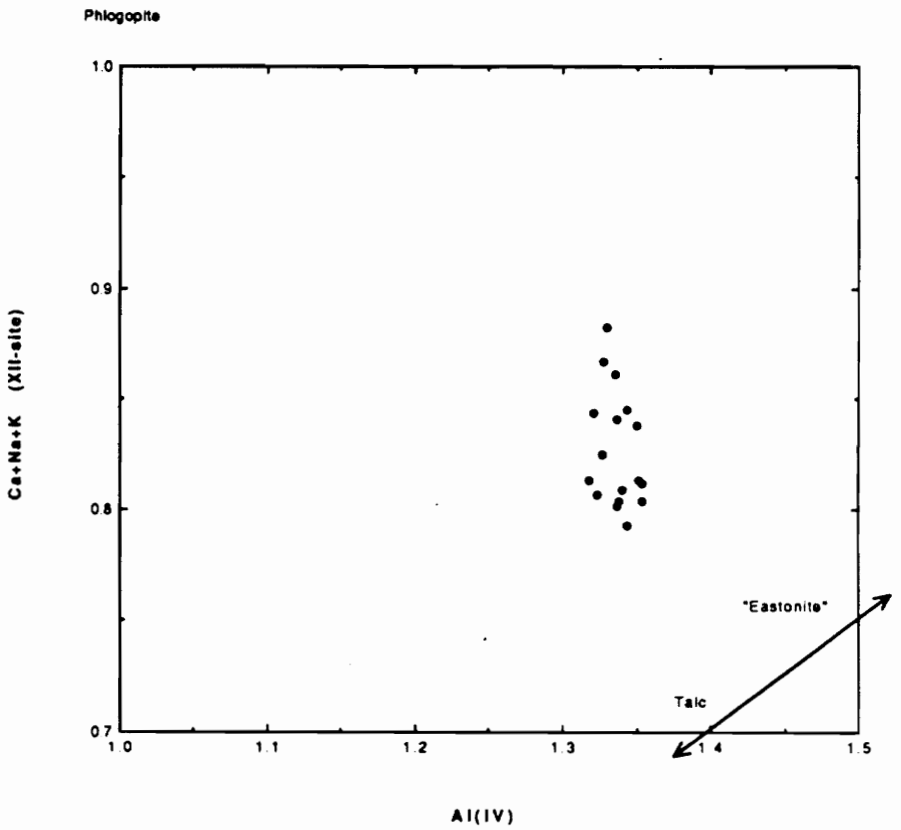

Figure 22. Expansion of boxed region in Figure 21 showing XII site occupancy *versus* Al^{IV} in biotite. See Text for discussion. After Dymek (1983).

the assumption of all ferrous iron is that data points plot lower on the positive charge axis than they otherwise would if the amount of ferric iron were known. Therefore, the value for total positive charge represents a minimum value. This lends support to the idea that some of the total iron is Fe^{3+}. Furthermore, the calculated XII-fold (interlayer) deficiencies would result in lowering the total positive charge.

Figure 21 shows that on a plot of $(Na+K+Ca)^{XII}$ *versus* Al^{IV}, all the data plot within the talc-phlogopite-"eastonite"[1] field. The data indicate that there is a talc component to these biotites, possibly related via substitution (17). Alternatively, the interlayer site deficiencies may be due to chloritization of biotite.

In a section above (see Petrography and Mineral Chemistry - Biotite), it was stated that the Ti content of biotite appears to be comparable to biotites of lower P-T terrains. This is unusual in that the general consensus is that the solubility of Ti in biotite increases with increasing temperature (Abrecht and Hewitt, 1988). Dymek (1983) suggested that vacancy formation in biotite creates a crystallographically favorable environment for increased Ti-substitution. Perhaps the fact that there does not appear to be as much Ti-substitution taking place could indicate that vacancy formation is not prevalent. Interaction between the Al-Tschermak substitution (13) and the Ti-Tschermak substitution (15) may significantly affect the amount of Ti in biotite. As Al^{IV} is substituted for Si^{IV}, the tetrahedral sites become larger and as Ti^{VI} is substituted for Mg^{VI} and Fe^{VI}, the octahedral sites become smaller. The combined effects of both (13) and (15) may tend to greatly increase the structural misfit between octahedral and tetrahedral layers and may have the ultimate result of discouraging Ti substitution at higher pressures because the structural misfit is too great for the biotite to be stable.

---

[1] "eastonite" is used here for simplicity to represent $KMg_2AlAl_2Si_2O_{10}(OH)_2$

The low K content is another concern because it may indicate chloritization which forces biotites to Mg-richer compositions, thus causing calculated peak temperatures and pressures to be lower than they actually should be. The low K content might be due to chloritization of the biotites or perhaps to substitution (17), which moves phlogopite-annite towards talc.

The ZnO content in staurolites analyzed in this study is quite variable (0.38 to 2.41 wt%). Guidotti (1970) stated that ZnO increases with metamorphic grade, based on the model that Zn^{2+} is preferentially concentrated in decreasing modal amounts of staurolite with increasing grade. The largest euhedral staurolites in this study (e.g. BR-2, TH-6A, TH-8, TH-10, and WAT-5) contain the lowest concentrations of ZnO, whereas the smallest anhedral resorbed staurolites contain the largest concentrations (e.g. CO-1A, CO-5, and TH-5B), and intermediate size staurolites contain intermediate ZnO concentrations (e.g. , TH-9, WAT-1A, and WAT-4). Results from this study are entirely consistent with Guidotti's (1970) observation.

P_{H_2O}/P_{total}

Figure 10 shows that P_{H_2O}/P_{total} is highest closest to the Waterbury Dome, and generally decreases with increasing distance from the dome. There is no apparent correlation between P_{H_2O}/P_{total} and anything that would indicate a greater progress of reaction. Rather, the higher ratios near the Waterbury Dome could be due to The Straits Schist acting as an aqueduct to channel water released from deeper level dehydration reactions to higher crustal levels.

A note of caution should be introduced here. There is a greater temperature dependence than compositional dependence on the fugacity (and hence pressure)

calculation. Therefore, any interpretations based on the P_{H_2O}/P_{total} ratios should be made with great care.

TECTONIC IMPLICATIONS

Results of this study give insight into relative cooling rates. It is generally accepted that any metamorphic garnet which has been heated to ≈650°C or above should be homogenized in composition due to the rapid increase in diffusion rates above 600°-650°C (Lasaga, 1983). Many of the rocks discussed here reached temperatures where zoning should not have been preserved if sufficient time was available for diffusional homogenization. The fact that apparent original growth zoning is present in garnets from The Straits Schist indicates that the rocks were probably essentially quenched, because rapid cooling kinetically inhibits reequilibration, and therefore should inhibit homogenization of the garnet. Rapid cooling is also suggested by the garnet Ca-zoning maps of Figures 4d and 5d, which show broken garnets with virtually no reequilibration effects along the broken edges that expose interior compositions.

These results are consistent with the work of Hames and others (1989) on post-Acadian cooling and unroofing. Their combined fluid inclusion and mineral equilibrium data indicate that parts of the Rowe-Hawley belt underwent rapid initial unroofing following high-pressure Acadian amphibolite-grade metamorphism. Their results indicate that the peak of metamorphism was about 390 Ma, with rocks at depths of about 30 km. Initially, the uplift rate averaged about 1.4 mm/yr and produced an average cooling rate of 13°C/my. At about 376 Ma, the rocks were at a depth of about 10 km. The rocks now continued in their uplift path, but at rates of about 0.1 mm/yr and produced an average cooling rate of 9°C/my.

Further tectonic implications have to do with the rather high pressures, indicating up to 30 km or more of post-Taconian overburden, either sedimentary or thrust-tectonic or both (Tracy and others, 1990).

REFERENCES

Abrecht, J. and Hewitt, D.A. (1980) Ti-substitution in synthetic Fe-biotites. (abstr.) Geological Society of America Abstracts with Programs, v. 12, p. 377.

Abrecht, J. and Hewitt, D.A. (1981) Substitutions in synthetic Ti-biotites. (abstr.) Geological Society of America Abstracts with Programs, v. 13, p. 393.

Abrecht, J. and Hewitt, D.A. (1988) Experimental evidence on the substitution of Ti in biotite. American Mineralogist, v. 73, p. 1275-1284.

Albee, A.L., and Chodos, A.A (1969) Minor element content of coexisting Al SiO polymorphs. American Journal of Science, v. 267, p. 310-316.

Armstrong, R.L., Barton, J.M., Carmalt, S.W., and Crowley, W.P. (1970) Geochronologic studies of the Prospect, Ansonia, and Milford formations, southern Connecticut. Contributions to Geochronology in Connecticut, I. Connecticut State Geologic and Natural History Survey Report of Investigations 5, p. 19-26.

Bohlen, S.R., Peacor, D.R., and Essene, E.J. (1980) Crystal chemistry of a metamorphic biotite and its significance in water barometry. American Mineralogist, v. 65, p. 55-62.

Bohlen, S.R., Wall, V.J., and Boettcher, A.L. (1983) Experimental investigations and geological applications of equilibria in the system FeO-TiO_2-Al_2O_3-SiO_2-H_2O. American Mineralogist, v. 68, p. 1049-1058.

Chatterjee, N.D. and Froese, E. (1975) A thermodynamic study of the pseudobinary join muscovite-paragonite in the system $KAlSi_3O_8$-$NaAlSi_3O_8$-Al_2O_3-SiO_2-H_2O. American Mineralogist, v. 60, p. 985-993.

Cheney, J.T. and Guidotti, C.V. (1979) Muscovite-plagioclase equilibria in sillimanite + quartz bearing metapelites, Puzzle Mountain Area, Northwest Maine. American Journal of Science, v. 279, p. 411-434.

Chinner, G.A., Smith, J.V., and Knowles, C.R. (1969) Transition metal contents of Al_2SiO_5 polymorphs. American Journal of Science, v. 267-A, p. 98-113.

Clark, G. and Kulp, J.L. (1968) Isotopic age study of metamorphism and intrusion in western Connecticut and southerastern New York. American Journal of Science, v. 266, p. 865-894.

Deer, W.A., Howie, R.A., and Zussman, J. (1962) *Rock-forming minerals, Ortho- and Ring Silicates*, Vol. 1. London: Longmans, p. 151-160.

Deer, W.A., Howie, R.A., and Zussman, J. (1966) *An Introduction to the Rock Forming Minerals*. London: Longmans., p. 201-205.

Dietrich, J.H. (1968) Multiple folding in western Connecticut: A reinterpretation of structure in the Naugatuck-New Haven-Westport area: Connecticut State Geological and Natural History Survey Guidebook 2, p. D-2, 1-13.

Dietsch, C. W., ms, (1988) The geology of the Waterbury dome, west-central Connecticut. Ph.D. dissertation, Yale University, 333p.

Dietsch, C.W. (1989) The Waterbury dome, west-central Connecticut: A triple window exposing deeply deformed, multiple tectonic units. American Journal of Science, v. 289, p. 1070-1097.

Dyar, M.D. (1990) Mossbauer spectra of biotite from metapelites. American Mineralogist, v. 75, p. 656-666.

Dymek, R.F. (1983) Titanium, aluminum and interlayer cation substitutions in biotite from high-grade gneisses, West Greenland. American Mineralogist, v. 68, p. 880-899.

Engel, A.E.J. and Engel, C.S. (1960) Progressive metamorphism and granitization of the major paragneiss, northwest Adirondack Mountains, New York, Pt. 2, Mineralogy. Geological Society of America Bulletin, v. 71, p. 1-58.

Evans, B.W. (1969) Chlorine and fluorine in micas of pelitic schists from the sillimanite-orthoclase isograd, Maine. American Mineralogist, v. 54, p. 1209-1211.

Evans, B.W. and Guidotti, C.V. (1966) The sillimanite-potash feldspar isograd in Western Maine, U.S.A. Contributions to Mineralogy and Petrology, v. 12, p. 25-62.

Ferry, J. M. and Spear, F.S. (1978) Experimental calibration of the partitioning of Fe and Mg between biotite and garnet. Contributions to Mineralogy and Petrology, v. 66, p. 113-117.

Foster, M.D. (1960a) Layer charge relations in the dioctahedral and trioctahedral micas. American Mineralogist, v. 45, p. 383-398.

Foster, M.D. (1960b) Interpretation of the compositions of trioctahedral micas. U.S. Geological Survey Professional Paper 354-B, p. 11-48.

Fritts, C.E. (1962) Age and sequence of metasedimentary and metavolcanic formations northwest of New Haven, Connecticut. U.S. Geological Survey Professional Paper 450-D, p. D32-D36.

Fritts, C.E. (1963) Bedrock geology of the Mount Carmel quadrangle, Connecticut. U.S. Geological Surevy Quadrangle Map 199.

Guidotti, C.V. (1970) The mineralogy and petrology of the transition from the lower to upper sillimanite zone in the Oquossoc Area, Maine. Journal of Petrology, v. 11, p. 277-336.

Guidotti, C.V. (1973) Compositional variation of muscovite as a function of metamorphic grade and assemblage in metapelites from N.W. Maine. Contributions to Mineralogy and Petrology, v. 42, p. 33-41.

Guidotti, C.V. (1984) Micas in metamorphic rocks. *In* Bailey, S.W., *ed.*, Mineralogical Society of America Reviews in Mineralogy, v. 13, p. 357-467.

Guidotti, C.V., Cheney, J.T., and Guggenheim, S. (1977) Distribution of titanium between coexisting muscovite and biotite in pelitic schists from Northwestern Maine. American Mineralogist, v. 62, p. 438-448.

Hall, L.M. (1976) Preliminary correlation of rocks in southwestern Connecticut. *In* Page, L.R., *ed.*, Geological Society of America Memoir 148, Contributions to the stratigraphy of New England, p. 337-349.

Hames, W.E., Tracy, R.J., and Bodnar, R.J. (1989) Postmetamorphic unroofing history deduced from petrology, fluid inclusions, thermochronometry, and thermal modeling: an example from southwestern New England. Geology, v. 17, p. 727-730.

Hatch, N.L., Jr. (1988) Some revisions to the stratigraphy and structure of the Connecticut Valley trough, eastern Vermont. American Journal of Science, v. 288, p. 1041-1059.

Hatch, N.L., Jr. and Stanley, R.S. (1973) Some suggested stratigraphic relations in part of southwestern New England. United States Geological Survey Bulletin 1380. 83 p.

Heinrich, Kurt F.J. (1981) *Electron Beam X-Ray Microanalysis*. New York: Van Nostrand Reinhold and Company, 578 p.

Hewitt, D.A. and Abrecht, J. (1986) Limitations on the interpretation of biotite substitutions from chemical analyses of natural samples. American Mineralogist, v. 71, p. 1126-1128.

Hess, P.C. (1969) The metamorphic paragenesis of cordierite in Pelitic Rocks. Contributions to Mineralogy and Petrology, v. 24, p. 191-207.

Hodges, K.V. and Crowley, P.D. (1985) Error estimation and empirical geothermobarometry for pelitic systems. American Mineralogist, v. 70, p. 702-709.

Hodges, K.V. and McKenna, L.W. (1987) Realistic propagation of uncertainties in geologic thermobarometry. American Mineralogist, v. 72, p. 671-680.

Hodges, K.V. and Spear, F.S. (1982) Geothermometry, geobarometry and the Al_2SiO_5 triple point at Mt. Moosilauke, New Hampshire. American Mineralogist, v. 67, p. 1118-1134.

Holdaway, M.J. (1971) Stability of andalusite and the aluminosilicate phase diagram. American Journal of Science, v. 271, p. 97-131.

Hollister, L.S. (1966) Garnet zoning: An interpretation based on the Rayleigh fractionation model. Science, v. 154, p. 1747-1651.

Koziol, A.M. and Newton, R.C. (1988) Redetermination of the anorthite breakdown reaction and improvement of the plagioclase-garnet-Al_2SiO_5-quartz geobarometer. American Mineralogist, v. 73, p. 216-223.

Kwak, T.A.P. (1968) Ti in biotite and muscovite as an indication of metamorphic grade in almandine amphibolite facies rocks from Sudbury, Ontario. *Geochemica et Cosmochemica Acta*, v. 32, p. 1222-1229.

Labotka, T.C. (1983) Analysis of the compositional variations of biotite in pelitic hornfelses from Northeastern Minnesota. American Mineralogist, v. 68, p. 900-914.

Lasaga, A.C. (1983) Geospeedometry: An extension of geothermometry. *In* Saxena, S.K., *ed.* Kinetics and Equilibrium in Mineral Reactions. New York: Springer-Verlag, p. 81-114.

Newton, R.C. and Haselton, H.T. (1981) Thermodynamics of the garnet - plagioclase-Al_2SiO_5-quartz geobarometer. *In* Newton, R.C., Navrotsky, A., and Wood, B.J., *eds.* Thermodynamics of Minerals and Melts. New York: Springer, p. 129-145.

Oki, Y. (1961) Biotites in metamorphic rocks. Contributions of the Geological Institute of Tokyo, p. 497-506.

Pigage, L.C. and Greenwood, H.J. (1982) Internally consistent estimates of pressure and temperature: the staurolite problem. American Journal of Science, v. 282, p. 943-969.

Rodgers, J., compiler (1982) Preliminary Bedrock Geologic Map of Connecticut. *In* Joesten, R. and Quarrier, S.S., *eds.*, New England Intercollegiate Geological Conference 74th Annual Meeting, Guidebook for fieldtrips in Connecticut and south central Massachusetts. Connecticut State Geologic and Natural History Survey Guidebook No. 5. Scale 1:250,000.

Rodgers, J., compiler (1985) Bedrock Geologic Map of Connecticut. Connecticut Geological and Natural History Survey. Scale 1:125,000. Two sheets.

Rodgers, J., Gates, R.M., and Rosenfeld, J.L. (1959) Explanatory text for the preliminary geological map (1956) of Connecticut. Connecticut Geological and Natural History Survey Bulletin 84, 64 p.

Seidemann, D.E. (1980) K-Ar and Rb-Sr dates for the Reynolds Bridge gneiss and a post-metamorphic Thomaston granite dike at Reynolds Bridge, western Connecticut. Contributions to Geochronology in Connecticut, II. Connecticut State Geological and Natural History Survey Report of Investigations 10, p. 5-12.

Silliman, B. (1820) Sketches of a tour in the counties of New-Haven and Litchfield in Connecticut, with notices of the geology, mineralogy, and scenery. American Journal of Science, 1st series, v. 2, p. 201-235.

Stanley, R.S. (1968) Metamorphic geology of the Collinsville area. *In* Orville, P.M., *ed.*, New England Intercollegiate Geological Conference 60th Annual Meeting, Guidebook for fieldtrips in Connecticut. Connecticut State Geological and Natural History Survey, Guidebook No. 2, p. D4-1-17.

Stanley, R.S. and Hatch, N.L., Jr. (1988) The pre-Silurian geology of the Rowe Hawley zone. *In* Hatch, N.L., Jr., *ed.*, The bedrock geology of Massachusetts. United States Geological Survey Professional Paper 1366. p. A1-A39.

Stout, M.Z., Crawford, M.L., and Ghent, E.D. (1986) Pressure-temperature and evolution of fluid compositions of Al_2SiO_5-bearing rocks, Mica Creek, B.C., in light of fluid inclusion data and mineral equilibria. Contributions to Mineralogy and Petrology, v. 92, p. 236-247.

Thompson, J.B. (1957) The graphical analysis of mineral assemblages in pelitic schists. American Mineralogist, v. 42, p. 842-858.

Thompson, A.B. (1976) Mineral reactions in pelitic rocks: II. Calculation of some P-T-X(Fe-Mg) phase relations. American Journal of Science, v. 276, p. 425-454.

Tracy, R.J. (1975) High grade metamorphic reactions and partial melting in pelitic schist, Quabbin Reservoir area, Massachusetts. Deparment of Geography and Geology, University of Massachusetts Contribution No. 20, 127 p.

Tracy, R.J. (1978) High grade metamorphic reactions and partial melting in pelitic schist, west-central Massachusetts. American Journal of Science, v. 275, p. 150-178.

Tracy, R.J. (1982) Compositional zoning and inclusions in metamorphic minerals. *In* Ferry, J.M., *ed.*, Mineralogical Society of America Reviews in Mineralogy v. 10, p. 355-397.

Tracy, R.J., Robinson, P.R., Thompson, A.B. (1976) Garnet composition and zoning in the determination of temperature and pressure of metamorphism, central Massachusetts. American Mineralogist, v. 61, p. 762-775.

Tracy, R.J. and Robinson, P.R. (1978) Metamorphic isograd mapping in central Massachusetts and the study of changing mineral compositions in metamorphism. Geological Society of America Abstracts with Programs, v. 10, p. 89.

Tracy, R.J., Hames, W.E., Miller, S.J., and Armstrong, T.R. (1990) Contrasting styles of Taconian, western Acadian, and eastern Acadian metamorphisms, south-central New England: Implications for Paleozoic tectonometamorphic evolution. Metamorphic Styles in Young and Ancient Orogenic Belts, Abstracts with Programs, University of Calgary, Calgary, Alberta, Canada.

Yardley, B.W.D. (1989) *An Introduction to Metamorphic Petrology.* New York: Longman Scientific and Technical, Longman Earth Science Series, 248 p.

VITA

Stephen John Miller was born October 16, 1966 in Murfreesboro, Tennessee. After spending time in Murfreesboro, Carbondale (Illinois), and Newark (Delaware), his family eventually settled in Oak Park, Illinois, where Steve grew up and matured. He graduated from Oak Park and River Forest High School in Oak Park in 1984 and proceeded to Bradley University in Peoria, Illinois. While studying Geological Sciences at Bradley, he was quite active in Delta Tau Delta International Fraternity, as well as Student Activities, the College of Liberal Arts and Sciences Dean's Advisory Council, and the Interfraternity Council. He earned his B.S. in Geological Sciences in 1988. Steve then ventured off to Southwestern Virginia to work on his M.S. in Geological Sciences at VPI and SU. While at VPI and SU, his activities outside Geological Sciences included volunteer work with the New River Valley AIDS Coalition (both Client Services and Education subcommittees), and in the Student Health Services AIDS Education committee and Peer Education program. He was also on the organizing committee of the Men's Health Clinic in Student Health Services.